

2020-10-03

# Role of dense shelf water in the development of Antarctic submarine canyon morphology

Gales, Jenny

<http://hdl.handle.net/10026.1/16486>

---

10.1016/j.geomorph.2020.107453

Geomorphology

Elsevier BV

---

*All content in PEARL is protected by copyright law. Author manuscripts are made available in accordance with publisher policies. Please cite only the published version using the details provided on the item record or document. In the absence of an open licence (e.g. Creative Commons), permissions for further reuse of content should be sought from the publisher or author.*

# Role of dense shelf water in the development of Antarctic submarine canyon morphology

J. Gales<sup>1\*</sup>, M. Rebesco<sup>2</sup>, L. De Santis<sup>2</sup>, A. Bergamasco<sup>3</sup>, F. Colleoni<sup>2</sup>, S. Kim<sup>4</sup>, D. Accettella<sup>2</sup>, V. Kovacevic<sup>2</sup>, Y. Liu<sup>5</sup>, E. Olivo<sup>2</sup>, E. Colizza<sup>6</sup>, C. Florindo-Lopez<sup>7</sup>, F. Zgur<sup>2</sup>, R. McKay<sup>8</sup>

(1)\* Biological and Marine Sciences, University of Plymouth, Plymouth, UK ([Jenny.gales@plymouth.ac.uk](mailto:Jenny.gales@plymouth.ac.uk))

(2) OGS, Borgo Grotta Gigante 42/C, 34010 Sgonico (TS), Italy

(3) Institute of Polar Science, CNR, Via Torino 155, 30172 Venezia, Italy

(4) KOPRI, 26 Songdomirae-ro, Yeonsu-gu, Incheon 21990, South Korea

(5) First Institute of Oceanography, Ministry of Natural Resources, China, Xianxialing Road 6, Laoshan

District, Qingdao 266061, China

(6) Department of Mathematics and Geosciences, University of Trieste, 34128 Trieste, Italy

(7) National Oceanography Centre, European Way, Southampton, SO14 3ZH, UK

(8) Antarctic Research Centre, Victoria University of Wellington, PO Box 600, Wellington 6140, New Zealand

**Keywords:** slope process, continental slope, submarine gully, meltwater

## 1. Abstract

Increased ocean heat supply to the Antarctic continental shelves is projected to cause accelerated ice sheet loss and contribute significantly to global sea-level rise over coming decades. Changes in temperature or salinity of dense shelf waters around Antarctica, resulting from increased glacial meltwater input, have the potential to significantly impact the location and structure of the global Meridional Overturning Circulation, with seabed irregularities such as submarine canyons, driving these flows toward the abyss. Submarine canyons also influence the location of intruding warm water currents by acting as preferential routes for rising Circumpolar Deep Water. These global changes have implications for large-scale effects to atmospheric and oceanic circulation. The ability for numerical modellers to predict these future behaviours is dependent upon our ability to understand both modern and past oceanic, sedimentological and glaciological processes. This knowledge allows ocean models to better predict the flux and pathways of Circumpolar Deep Water delivery to the shelf, and consequently to ice shelf cavities where melt is concentrated. Here we seek to understand how dense shelf water and other continental slope processes influence submarine canyon morphology by analysing newly

collected geophysical and oceanographic data from a region of significant and prolonged dense shelf water export, the Hillary Canyon in the Ross Sea. We find that cascading flows of dense shelf water do not contribute to significant gully incision at the shelf edge during interglacial periods, however, are strong enough to prevent gully infilling and contribute to canyon-levee aggradation down-slope. We find buried paleo-gullies beneath gullies incising the modern seafloor. Paleo-gullies occur as single gullies and in complexes indicating that gully activity was continuous over multiple glacial cycles and formed an important role in the development of the shelf edge and upper slope. Glacial cycles likely drive large-scale shifts in canyon head processes with periods of intense seafloor erosion and significant gully incision likely occurring when ice grounded near to the shelf edge, during glacial and deglacial periods, when sediment-laden subglacial meltwater was released at the shelf edge. We put slope morphology observed at the Hillary Canyon head into global perspective to show that cascading flows of dense shelf water do not exert consistent patterns of erosion on high-latitude continental margins.

## **2. Introduction**

Increased ocean heat supply to Antarctic continental shelves is projected to cause accelerated ice sheet loss and contribute significantly to global sea-level rise over coming decades to centuries (De Conto et al., 2016; IPCC, 2019). Currently, numerical modelling studies lack necessary resolution and spatial coverage of seafloor morphology data to sufficiently constrain past and future sub-ice shelf melting, ice-sheet collapse, and sea level change estimates (Petrini et al., 2018; Colleoni et al., 2018). This is because one of the major causes of current Antarctic ice sheet retreat stems from increased ocean heat supply to the continental shelves surrounding Antarctica, with atmospheric temperature rise contributing to a lesser extent (Rignot et al., 2019; IPCC, 2019). Recent studies show that heat and volume transport around Antarctica are substantially enhanced where seafloor irregularities, such as submarine canyons, allow dense shelf waters to descend down-slope (Morrison et al., 2020). Warm water incursions onto the shelf can be intermittent and highly localised and can vary depending on the geometry of the ice shelf and seafloor bathymetry (Padman et al., 2018). Lack of necessary resolution and data availability to image these irregularities therefore makes predictions and future estimates of ice sheet and oceanic changes difficult. Thinning of ice shelves, due to increasing ocean temperatures and warm water incursions can lead to rapid ice retreat. This is especially true where marine based ice-sheets occur in conjunction with a landward sloping seabed, seen around the West and East Antarctic Ice Sheet (WAIS and

EAIS, respectively) (Joughin et al., 2011). This fast ice-shelf retreat can lead to an overall disintegration of the marine-based section of ice-sheets.

Dense shelf water around Antarctica is produced predominantly in the Weddell and Ross Sea polynyas where seabed irregularities, such as canyons and basins, can drive these flows from the shelf to the deep ocean where mixing with ambient water drives the global Meridional Overturning Circulation (Jacobs et al., 2002; Purkey and Johnson, 2010). Changes in temperature or salinity of these waters, such as due to increased meltwater input from ice sheets and seasonal sea ice melt, lead to significant changes to the Meridional Overturning Circulation (Jacobs et al., 2004; Seidov et al., 2001; Weaver et al., 2003; Seidov et al., 2005). Recent studies show that freshening of bottom waters is already occurring in the Ross and Weddell seas due to factors such as increased ice mass loss in the Antarctic Peninsula and Amundsen Sea (Silvano et al., 2018). This has significant global implications for large-scale effects to ocean and atmospheric circulation, with changes to the strength of the Meridional Overturning Circulation potentially leading to abrupt and global climate changes (Ramhstaf, 1994; Manabe and Stouffer, 1995). Understanding the influence that dense shelf water has on seafloor morphology and vice versa has important implications for determining how these processes changed in the past, in response to different climatic conditions and ice sheet configurations on the continental shelf, and how ice sheet configuration may change in the future. Submarine canyons influence the location and dynamics of intruding warm waters that enhance melting and ice shelf retreat with dense shelf water cascading driving net onshore heat and volume transport of warm currents around Antarctica (Dinniman et al., 2003; Morrison et al., 2020). Thus, understanding how canyon morphology and isobath curvature evolved through time is crucial in understanding factors, processes and feedbacks contributing to past and future ice sheet retreat.

Ice-ocean interactions are arguably the most poorly constrained aspect of ice sheet, ocean and climate models. Extensive Antarctic paleo-climate records are recovered from the flanks of canyons or drifts associated with sediment delivery down-canyon (e.g. Rebesco et al., 2007; Barker and Camerlenghi, 2002), yet very little is known about canyon process across modern, as well as glacial-interglacial timescales. Understanding large-scale oceanic feedbacks as well as the differences in amplitude and frequency of Antarctic continental slope processes under different climatic conditions, noted in far-field paleo-oceanographic records, is essential for constraining how ice sheet and oceanic interactions may change in the future (e.g. Zachos et al., 2001).

Understanding the dynamics of processes operating in submarine canyons more widely is of global importance. This can improve understanding of hazards such as turbidity currents which transport the greatest sediment

volumes on earth (Talling et al., 2014). These flows have significant influence on the global carbon flux (Galy et al., 2007) and can influence shelf and deep-sea ecosystems through supplying nutrients (Canals et al., 2006). They contribute to continental margin and fan construction and aid transportation of pollutants to the deep-sea (Nilsen et al., 2008). On glaciated margins, canyons are not ubiquitous as on low latitude margins and are particularly rare on certain margins (Rui et al., 2019). Their study contributes to a better understanding of the dynamics of ice buildup and retreat and associated glacigenic sediment transport which is crucial in understanding the spatial and temporal variability of glacimarine and oceanographic processes operating on high-latitude margins.

We investigate how dense shelf water influences submarine canyon morphology by analysing new geophysical and oceanographic data from a region of significant and prolonged dense shelf water export, the Hillary Canyon in the Eastern Ross Sea, Antarctica (Fig. 1) (Bergamasco et al., 2002; Orsi et al., 2009; Morrison et al., 2020). We present a quantitative analysis of the main morphological features at the Hillary Canyon head, including gullies incising the modern seafloor and buried paleo-gullies and discuss processes influencing their distribution and formation. We discuss the ability for dense shelf water to influence canyon morphology and the modern and past implications of this before discussing the effects of dense shelf water around Antarctica and other high-latitude continental margins more widely.

### **3. Study Area**

The Hillary Canyon is a 180 km long, non-shelf incising canyon on the Eastern Ross Sea continental margin, Antarctica (Fig. 1). The morphology of the canyon is largely unknown due to a paucity of seafloor hydrographic data with much of the seafloor lacking sufficient resolution data. The continental shelf landward of the Hillary Canyon spans ~300 km to the modern front of the Ross Ice Shelf and is dissected by numerous deep, glacially carved troughs. The canyon lies at the mouths of two of those glacial troughs, the Pennell Trough and Glomar Challenger Basin, that were occupied by ice streams over multiple glacial cycles (Cooper et al., 1991; De Santis et al., 1995; Anderson et al., 2014; Halberstadt et al., 2016; Bart and Owolana, 2012). Grounded ice from the WAIS reached the shelf edge in the Eastern Ross Sea periodically since the Miocene and is thought to have last retreated during the Holocene (e.g. Anderson and Bartek, 1990; De Santis et al., 1995; McKay et al., 2016; Anderson et al., 2019).

The Ross Sea lies on the Western Antarctic Rift System and consists of three major sedimentary basins that formed during the break-up of Gondwana during the Late Cretaceous due to crustal extension and thinning

(Cooper et al., 1991). The basins are filled with eight major sedimentary packages following subsidence and deposition of prograding subglacial and glacial marine sedimentary packages with the oldest dated package (upper RSS-1) dating to the upper Eocene – Oligocene period (Traube and Zayatz, 1993; Brancolini et al., 1995; De Santis et al., 1995). To the east, the eastern Ross Sea Trough Mouth Fan forms a major sediment depocenter at the shelf edge seaward of the Glomar Challenger and the Whales Deep Basins likely dating to the Pliocene-Pleistocene (Alonso et al., 1992; Bart et al., 2000). The fan is characterised by outward-bulging contours with seismic data showing progradation of the margin. To the west of the Hillary Canyon, the Iselin bank forms a distinct topographic barrier with steep flanks.

The Hillary Canyon is a major conduit for Ross Sea Bottom Water (Bergamasco et al., 2002; Orsi and Wiederwohl., 2009; Morrison et al., 2020) contributing to Antarctic Bottom Water exported from the Ross Sea. Dense shelf water forms through sea ice formation and subsequent brine rejection and heat loss. High Salinity Shelf Water (characterised by salinity values of 34.75 to 34.85 psu; Jacobs et al., 1985) and Ice Shelf Water (characterised by temperatures below freezing due to supercooling beneath the Ross Ice Shelf) mix with ambient water (predominantly modified Circumpolar Deep Water; mCDW) forming dense shelf water (Bergamasco et al., 2002). Circumpolar Deep Water (CDW) can intrude onto the Ross Sea shelf and mix with shelf waters, where it forms mCDW (Budillon et al., 2011). These shelfward intrusions are enhanced, amongst other factors, by the presence of seafloor depressions, such as the Hillary Canyon (Dinniman et al., 2003). Oceanographic and modelling studies show that dense shelf water moves toward the shelf break along seafloor depressions and flows from the shelf to the abyss (Bergamasco et al., 2002; Budillon et al., 2011; Morrison et al., 2020).

#### **4. Methodology**

Geophysical and oceanographic data were collected in austral summer 2017 by R/V OGS Explora during the EUROFLEETS-funded ANTSSS expedition. The geophysical data covers 1575 km<sup>2</sup> at the Hillary Canyon head. Data were collected using a Reason SeaBat 7150 multibeam echosounder with an operating frequency of 12 kHz and swath width of 150°. Data were processed using PDS2000 to 50 m grid size. A Benthos Chirp III collected acoustic sub-bottom profiler data (frequency range 2-7 kHz; maximum ping rate 15 Hz). Single-channel seismic data were acquired over 453 km. The system was configured with a linear array of two 210 cu.in GI guns spaced 2 m apart and towed 4 m below the surface. Both guns were shot in harmonic mode (105 G + 105 I) with a shotpoint interval of 7-8 seconds (~13-15 m at 3.5-3.8 knots). The receiver was a 10 m solid state streamer with 10 channels towed 1-1.5 m beneath the surface. The near offset distance was 40 m. Data

were processed using Schlumberger Vista v.7 software following conventional seismic processing sequences, including quality control checks, amplitude recovery, bandpass filtering, 10 trace common shot domain stacking, signal enhancement using FX deconvolution (Gales et al., 2017).

Oceanographic data were collected by an Acoustic Doppler Current Profiler (ADCP), lowered (L-) ADCP, expendable BathyThermograph (XBT) and Conductivity-Temperature-Depth (CTD) SBE911plus probe which was equipped with optical backscattering and fluorescence sensors. An RDI Ocean Surveyor 75 kHz vessel mounted ADCP was configured with a 30° beam angle (4 beam phased array) with a maximum ping rate of 75 kHz and maximum operational range of 550 m to record horizontal water velocity. 20 XBT (Sippican Lockheed) probes were launched at the Hillary Canyon head. The XBTs had a sampling rate of 10 Hz, vertical resolution of 60 cm and temperature resolution of 0.01°C. Eight CTD casts recorded at a sampling frequency of 24 Hz and were averaged into 1 dbar bins. A Workhorse Sentinel Lowered-ADCP with a frequency of 300 kHz was attached to the water sampler frame.

Gully parameters were extracted from along-slope profiles 50 m below the shelf edge. Measured parameters included gully length (distance that gully can be traced down-slope), gully width (distance between points of maximum curvature of gully flanks), gully relief (vertical distance from maximum gully incision to line defining gully width), gully steepness (ratio between gully depth and width), gully sinuosity (measure of ratio of channel length vs straight-line distance of gully start to end) and cross-sectional shape to determine whether the profile is U-shape (parabolic) or V-shaped, measured using the General Power Law programme (SM. Fig.1; Pattyn and Van Hiele, 1998). Paleo-gully parameters including width and relief were extracted from seismic line IT17RS305B. Relief estimates were based on a constant velocity estimation of 1650 m/s taken from compressional P-wave velocity measurements from borehole U1523 located on the upper Ross Sea slope (McKay et al., 2019).

Grain size analysis was used to assess surficial sediment on the upper slope of the Eastern Ross Sea. Grain size measurements were carried out on box core RS14-BC3 (40 cm recovery) and gravity core RS14-C3 (275 cm recovery) collected in 2014 on R/V Italica in the frame of the RNRA ROSSLOPE-2 Project on the upper slope of the Eastern Ross Sea in 1214 m and 1215 m water depth respectively (Fig. 1). Samples were prepared in 1 cm thick intervals and treated with hydrogen peroxide to remove organic matter. Wet sieving separated gravel (> 2mm) and a Malvern Particle Size analyser was used with the addition of sodium polyphosphate (for dispersion) for the fine grain size analysis to obtain volume measurements of sand-silt-clay where sand (63 µm - 2 mm), silt

(2  $\mu\text{m}$  - 63  $\mu\text{m}$ ) and clay (< 2  $\mu\text{m}$ ) grain size boundaries are used. The maximum grain size able to be measured by the Malvern particle size analyser is 2 mm, therefore a clast count was also conducted to assess the coarse fraction (>2 mm) using wet-separation of the gravel (>2mm) component and X-rays of the cores.

## **5. Results**

### **5.1. Shelf-edge and canyon morphology**

The Hillary canyon head spans ~85 km along the shelf edge of the Eastern Ross Sea. The outer shelf is predominantly landward-deepening at the mouth of the Glomar Challenger Basin (from ~175°5'W to ~176°45'W). In the Pennell Basin, most of the shelf deepens landward, with the very outer shelf sloping seaward due to the presence of a sill at the mouth of the trough (west of ~176°45'W). The continental slope at the Glomar Challenger Basin mouth is characterised by an average slope gradient of ~3.5° with concave-upward profile to ~1500 m depth (d-d' in Fig. 1). Below this the canyon thalweg is relatively linear. At the mouth of the Pennell Trough, slope gradient increases to ~4.5°. To the east, the Eastern Ross Sea Fan forms a convex-outward depocenter seaward of the Glomar Challenger Basin with slopes <3°. Although data is limited here, widely spaced gullies occur on the outer-shelf and upper-slope of the fan. On the western fan flank, a small slide-scar (~18 km<sup>2</sup>) occurs that is ~11 km long, with a relief of ~30 m. Small blocks, ranging between 0.6 and 6 km in length, occur within the slide scar (Fig. 2). Oblique seismic profiles crossing the upper Hillary canyon (Fig. 2) and the lower part of the Ross Sea Fan western flank, show chaotic seismic units, with discontinuous, sub-horizontal reflectors onlapping the paleo-continental slope (Fig. 2C). Convex-shaped and opaque lenses lie at the base of the continental slope (Fig. 2C).

At the Glomar Challenger Basin mouth (~175°47'W), the shelf edge is incised by deep gully systems, covering ~55 km along-slope. The 49 gullies that incise the shelf edge are relatively straight, narrow and mostly non-branching, with average reliefs of 40 m, widths of 0.85 km and lengths of 4.5 km (Fig. 3, 4). The gullies have an average sinuosity of 1.3 (where 1 = straight and >1 indicates increasing sinuosity). The gullies have a cross-section shape of 0.9, indicating a V-shaped cross section (where values <1 indicate convex upward gully flanks and values >2 indicate a parabolic or box-shaped morphology; Pattyn and Van Huele, 1998). The gullies are predominantly wider, longer and steeper and are more widely spaced toward the Eastern Ross Sea Fan (175°30'W) where slope gradients are less steep (~3.5°). The gullies increase in frequency, density and steepness and decrease in width and length further westward where slope gradient increases to ~4.5°. A distinct lack of



gullies is observed at the mouth of the Pennell Trough (from 177°43'W) over ~30 km where the seafloor is relatively smooth and homogenous.

Sub-bottom profiler and single-channel seismic data collected parallel to the shelf edge show that the gullies incise the seafloor rather than being formed by aggrading gully levees (Fig. 3D, E). The gullies incise several parallel reflectors; many terminating above a strong parallel reflector we term R1 that shoals to sub-crop at the seabed toward the Pennell Trough (Fig. 3B). Beneath R1, numerous paleo-gullies are observed in the region of surface gullies, with no expression of paleo-gullies further westward at the Pennell Trough mouth (Fig. 3C). Most of the paleo-gullies have U-shaped cross-sections and occur in vertically stacked complexes, or as isolated occurrences. There are multiple generations of paleo-gullies that cut down from different horizons. Although some paleo-gullies follow the same pathway to surface gullies, incising in similar spatial locations but at greater depths, there are multiple occurrences of paleo-gullies initiating in regions absent of surface gullies. The seismic character of the paleo-gully fill is slightly brighter than the surrounding sediments, with a less chaotic nature. A series of smaller paleo-gullies occur along reflector R1, compared to the gullies incising the modern seafloor, with average reliefs of 28 m and widths of 0.24 km. Below R1, the paleo-gullies are significantly greater in relief compared to gullies incising the seafloor, with average reliefs of 154 m and widths of 0.65 km. No levees are observed in the seismic data indicating that the paleo-gullies are incisional. Further west, the subsurface is characterised by lens-shaped semi-transparent packages that pinch out toward the axis of the canyon (Fig. 3B).

The gullies converge with shallow channels around 1000 m water depth (Fig. 3A). The channels are U-shaped in cross-section and are wider (average 2.3 km wide) and shallower (average 13 m relief) than the shelf-edge gullies. The channels converge towards the main canyon axis which narrows and deepens down-slope, with a relief of ~400 m and width of ~45 km at 2400 m water depth (Fig. 1C). Seismic data show that the canyon here is deeply entrenched with large levees either side of the canyon thalweg (Fig. 5). The levees are characterised by continuous horizontal reflectors and are asymmetric with the eastern levee significantly larger with onlapping and depositional strata. The flanks of the main canyon thalweg are characterised by gullies and small-scale mass-wasting (Fig. 5).

## **5.2. Oceanographic observations**

Oceanographic observations at the Hillary Canyon head, collected in austral summer 2017 over a 3-week interval, show sustained high-velocity flows of cold, dense, bottom currents with velocities reaching ~1.0 m/s (Fig. 6). Over this interval, the highest velocity (~1.1 m/s) and coldest flows (~-1.5°C) were observed to the

west of the Hillary Canyon head, at the mouth of the Pennell Trough, in a region of homogenous seafloor absent of gullies. Although the flow may be quite variable in time and space, the predominant direction of the currents during the observed interval was off the continental shelf, toward the canyon axis (Fig. 6C), in agreement with previous measurements showing energetic bottom currents present all year round (Bergamasco et al., 2002; Budillon et al., 2011). Further east, toward the mouth of the Glomar Challenger Basin, shipboard ADCP data show a decrease in current velocity, although direction remains predominantly constant off the continental shelf (Fig. 6B, C). Here, XBT profiles show temperature is slightly higher ( $\sim 0.5^{\circ}\text{C}$ ) near seafloor compared to the Pennell Trough mouth (Fig. 6A).

The CTD probe data (Fig. 7A) show the vertical structure of the water column west of the Hillary Canyon head. The profiles show the presence of cold ( $\sim -0.8^{\circ}\text{C}$ ), low salinity ( $\sim 34.1$  PSU) water near the surface with high levels of turbidity ( $\sim 0.14$  NTU) and fluorescence ( $\sim 1.5$   $\text{mg}/\text{m}^3$ ). Warm and saline waters lay beneath, in the intermediate layers. Near the seafloor, salinity decreases slightly, and temperature decreases significantly to  $\sim 34.6$  PSU and  $\sim -1.3^{\circ}\text{C}$  showing the signature of Ice Shelf Water. Fluorescence remains very low at the seafloor ( $< 0.5$   $\text{mg}/\text{m}^3$ ). In all CTD casts, turbidity values increase toward the seafloor to  $\sim 0.12 - 0.13$  NTU. L-ADCP transects show a significant increase in current velocity toward the seafloor at stations 2, 5 and 6, with velocity nearing  $1.1$  m/s (Fig. 7B).

### 5.3. Grain size measurements

Grain size measurements from box core RS14-BC3 and gravity core RS14-C3 from the Ross Sea mid slope at  $\sim 1214$  m water depth (Fig. 1) show surficial (upper 6 cm RS14-BC3; upper 25cm RS14-C3) sediments of sandy silt with gravel clasts and silty clay dominating beneath (7-37 cm RS14-BC3; 29-271 cm RS14-C3; SM.Fig.2). A sandy interval occurs between 44-45 cm of RS14-C3 (43% sand). Ice rafted debris, as indicated by gravel grains ( $> 2\text{mm}$ ), decrease in the top of core RS14-BC3 to 4 cm before increasing to peak at 8 cm (11 counts), 17 cm (20 counts) and 37 cm (20 counts) core depth.

## 6. Discussion

In this section we discuss new geomorphic, sub-surface and oceanographic results from the Hillary canyon in relation to the glacial, oceanographic and sedimentary processes influencing canyon morphology. We discuss the influence of dense shelf water on gully morphology more widely and compare characteristics of submarine gullies observed on other high-latitude continental margins.

## 6.1. Influence of grounded ice extent on continental slope morphology

The distribution of gullies incising the seafloor along the Eastern Ross Sea margin correspond with the maximum extent of grounded ice during the Last Glacial Maximum (Fig. 8). Geomorphological and sedimentological reconstructions show that ice advanced across the Eastern Ross Sea shelf during glacial periods, although timing and extent was not homogenous (e.g. Shipp et al., 1999; Bart and Owolana, 2012; Anderson et al., 2014; Halberstadt et al., 2016; Prothro et al., 2020). At the mouth of the Glomar Challenger Basin, large, V-shaped and deeply incised gullies occur. Here, multibeam echosounder data show the presence of well-defined megascale glacial lineations occurring up to near the shelf edge indicating that ice streams reached the shelf edge (Shipp et al., 1999; Halberstadt et al., 2016). By contrast, a distinct lack of gullies is observed at the mouth of the Pennell Trough over ~30 km along-slope. The presence of a large grounding zone wedge occurs 120 km landward of shelf edge and north of this there are no well-defined megascale glacial lineations suggesting that ice did not extend to the shelf edge here since the Last Glacial Maximum (although multibeam echosounder data here are very sparse compared to the Glomar Challenger Basin) (Fig. 8; Halberstadt et al., 2016). This configuration is also suggested by age and sedimentology of available sediment cores (Prothro et al., 2018; 2020). A single multibeam swath shows megascale glacial lineations on the northwestern flank of the bank dividing the Pennell Trough from the Glomar Challenger Basin indicating grounded ice flow parallel to the Pennell Trough axis (Prothro et al., 2018; 2020). These lineations do not reach the shelf edge but terminate against the morainal ridge lying at the shelf edge and closing the Pennell Trough mouth, suggesting that grounded ice did not reach the shelf edge or that glacial lineations have been completely reworked by iceberg keels after ice retreat (Fig. 8).

The extent of grounded ice across the continental shelf impacts slope processes and thus gully incision. Grounded ice transports large volumes of unsorted sediments to its margins particularly through ice streams (Golledge et al., 2011). At the Glomar Challenger Basin mouth, seismic data show a prograded continental margin (Fig. 2B, C) providing evidence for a prolonged history of ice advance and sediment delivery to the shelf edge over much of the Neogene and Quaternary (Cooper et al., 1991; De Santis et al., 1995, Anderson et al., 2019). Sediment failures are observed in recent and older strata along the continental slope (Fig. 2B, C). Along the margin at the mouth of the Glomar Challenger Basin, chaotic seismic units are observed with discontinuous, subhorizontal reflectors onlapping the paleo-continental slope, suggesting that sliding processes occurred during past margin progradation, or between periods of margin build out (Fig. 2C). Convex-shaped, opaque, lenses at

the base of the continental slope indicate repeated episodes of mass transfer gravity flows and channel-levee turbiditic construction (Laberg and Vorren, 1995) (Fig. 2C). Small slide scars also occur on the present day seabed on the western flank of the Eastern Ross Sea Fan, with small blocks interpreted as slide blocks or relict seafloor within the slide scar (Fig. 2). Although these slides may have been triggered following LGM and previous glacial maxima, the slides were likely influenced by ice loading. Grounded ice can lead to rapid deposition of sediment causing under-compaction of the slope and increase in pore pressure; formation of weak layers, where failure occurs within weaker interglacial substrate sediments (e.g. contouritic, plumitic, hemipelagic, diatomaceous layers) with excess pore water pressure caused by loading by stiffer glacial sediments rapidly deposited during glacial conditions and loading / unloading of ice at the shelf break (e.g. Melles and Kuhn, 1993; Dugan and Flemings, 2000; Laberg & Vorren 2000; Long et al., 2003; Volpi et al., 2003; Maslin et al., 2004; Donda et al., 2008). These slope failures may result in sediment and water mixing to generate turbidity currents explaining erosion further down-slope e.g. where debris flows transition to erosive turbidity currents (Fig. 9B) Piper et al., 1999; Talling et al., 2014).

Ice sheet grounding affects the structure and physical properties of the shelf edge and controls sediment distribution and associated margin architectural changes that influence the occurrence of mass-wasting processes (Vorren et al., 1998; Long et al., 2003). The high-volume of sediment delivery associated with advancing grounded ice can precondition the slope to down-slope processes such as turbidity currents which can cause seafloor erosion (Damuth et al., 1978; Vorren et al., 1998; Laberg and Vorren, 2000). Moreover, sediment supplied at the mouth of glacial troughs tends to have lower shear strength as a consequence of shear remoulding, under-compaction and sorting produced by meltwater, thus facilitating mass movements and subsequently a lower gradient of the continental slope (Rebesco et al., 1998). In addition, not only the amount of sediment delivery, but also its distribution and subsequent margin architectural changes (associated with changes in the glacial thermal regimes) control the occurrence of failure episodes and mass-wasting processes (Diviacco et al., 2006; Rebesco and Camerlenghi, 2008). The importance of slope preconditioning has been observed in other glacial and non-glacial environments where sediment availability has been shown to be a crucial factor in processes such as turbidity current generation where dilute flows can mobilise accumulations of fine sediments (e.g. Vorren et al., 1998; Hage et al., 2019; Normandeou et al., 2019; Pope et al., 2019).

Grounded ice can influence the availability of subglacial and ice front meltwater (discussed in section 6.3).

These effects are modified by specific characteristics of the study area, such as the underlying geology which

affects seabed erodibility, deformation and thus ice flow, slope geometry and gradient, glacial history, drainage basin size and climate history (e.g. Rebesco et al., 1998; Ó Cofaigh et al., 2003; Wynn et al., 2012).

## **6.2. Can dense shelf water cause gully erosion?**

Oceanographic observations show that over a 3-week period, cold, dense waters move toward the canyon head, reaching speeds of ~1 m/s near to the seafloor. Gullies are absent from the region of most energetic cascading flows. This follows previous in-situ observations (e.g. CLIMA project; Bergamasco et al., 2002; Petrelli et al., 2008) from the shelf break and numerical modelling studies that show the Hillary Canyon to be a major region of cascading dense shelf water with waters driven to the west of the canyon by Coriolis (Fig. 6; Budillon et al., 2011; Morrison et al., 2020). We use bed shear stress ( $\tau\theta$ ; equation [1]) to assess the current's ability to erode the seafloor, where  $C_d$  is the friction factor,  $\rho$  is water density and  $u$  is depth averaged flow speed (SM.Table 1).

$$\tau\theta = C_d \rho u^2 \quad (1)$$

Under the observed modern austral summer conditions, bottom currents are great enough to initiate sediment motion. Calculations of bed shear stresses associated with observed currents ( $\tau\theta = 2.57$  Pa) show that these currents are able to erode marine muds (0.05-2 Pa) and sandy muds (0.1-1.5 Pa) (McCave, 1984; Jacobs et al., 2011) which dominate interglacial sediment supplied to the slope via iceberg rafting, along-slope currents, glaciomarine and hemipelagic, pelagic and biogenic settling (e.g. Vanneste and Larter, 1995; Rebesco et al., 1996). Sediment trap deployments on the outer Ross Sea shelf show that the modern vertical flux is dominated by faecal pellets and aggregate particles with equivalent stokes sphere sizes of 59 $\mu$ m-96 $\mu$ m (Jaeger et al., 1996). There is no information about seabed sediment on the steep upper slope where dense water flows reach highest velocity in present time. However, recent box (RS14-BC3) and gravity core (RS14-C3) grain size measurements from the Ross Sea mid slope (Fig. 1) show surficial interglacial sediments of sandy silt (SM.Fig. 2), from which the fine silt fraction component was likely removed and the coarse sediment (IRD) sorted by bottom currents. Considering that the observed along-slope and down-slope currents are fastest on the upper slope (Fig. 6), they are less able to erode glaciogenic sediments which have much higher critical shear stresses that form the bulk of the mid slope cores beneath surficial interglacial sediments (e.g. 2.2-23 Pa; Pike et al., 2018). The glaciogenic sediments are characterized by increased clay content, low sand content and increased Ice Rafted Debris (Lucchi et al., 2002; Fig.1; SM.Fig.2). At the shelf edge, the currents can initiate suspension of recent sediment, and thus

maintain gully morphology avoiding significant sediment infilling, however, are unlikely to erode glacial sediments present.

Our observations suggest that under modern conditions, erosion of gullies is not likely to be dominated by flows of cascading dense shelf water as gullies are absent from the region of most energetic and sustained dense shelf water overflow (Bergamasco et al., 2002; Morrison et al., 2020). Recent in-situ direct monitoring experiments of very dilute plumes in other ice-marginal settings show that dilute plumes can generate turbidity currents if the seafloor is sufficiently preconditioned e.g. if sediment is allowed to build up between resuspension events (Hage et al., 2019). The movement of sediment by dense water cascading differs from turbidity currents in that dense water cascading is gravity-driven, where the descending movement of dense water entrains sediments, as opposed to turbidity currents where it is the movement of loose sediment that entrains water movement (Canals et al., 2006). Although the ability for dense shelf water to entrain sediment and produce gravity flows is poorly understood (Canals et al., 2006; Talling et al., 2014), sustained accumulations and subsequent resuspension events of biogenic and fine-grained particles at the Hillary canyon head could condition the slope for potential sediment gravity flows. The Ross Sea has moderate rates of modern primary productivity in the upper 100 m of the water column (e.g. Jaeger et al., 1996; Smith et al., 1996). Under modern conditions, if sediments supplied to the outer shelf / upper slope were able to accumulate over prolonged periods of time, such as between major dense shelf water cascading events (e.g. via iceberg rafting, along-slope currents, glaciomarine, hemipelagic, pelagic and biogenic settling), movement of sediment and concentration may become sufficient to generate sediment gravity flows if triggered by some external mechanism e.g. earthquake or glacial earthquake, glacio-isostatic adjustment, wave loading, internal waves and tides, energetic tidal jets, landslides, energetic dense water cascade or release of sediment-laden subglacial meltwater (Palanques et al., 2009; Talling et al., 2014; Clare et al., 2016; Maier et al., 2019; Nettles and Ekström, 2010).

The Eastern Ross Sea is a passive margin, therefore less likely to be affected by tectonic influences such as earthquakes, although glaciotectonic processes may occur during glacial retreat (Lee and Philips et al., 2013). Most of the continent is permanently covered in ice and the canyon is located >300 km from the modern ice front, therefore sediment resuspension cannot be associated with river discharge. The shelf-edge currently lies at ~570 m water depth therefore is not directly affected by surface waves and storms, although internal tides and waves are known to occur throughout this region (Robertson et al., 2003) thus may become important if current velocity is enough to resuspend sediments (e.g. Maier et al., 2019). Intense meteorological events on glaciated

margins may control the production of dense shelf water plumes, which can resuspend significant amounts of sediment (Bensi et al., 2019). Where sediment can build up between resuspension events, exceptionally strong and persistent episodes of dense shelf water cascading could increase sediment movement and concentration enough to produce sediment gravity flows down slope. This could result in sediment transport down-canyon, although these low-density flows are unlikely to cause significant gully erosion (Fig. 9A).

Under full-glacial conditions, where grounded ice extended to the shelf edge, the formation of Ice Shelf Water and High Salinity Shelf Water directly over the continental shelf was likely impeded as no or very little sea ice was able to form on the continental shelf due to increased grounded ice extent. This limits the delivery of salt required for dense water formation, minimising dense shelf water developing and cascading over the shelf edge. Sea ice and brine rejection could, however, continue to form seaward of the ice margin over the continental slope. Following glacial retreat from the shelf edge (e.g. during deglaciation), dense shelf water cascading likely resumes due to sea ice reforming over the continental shelf and Ice Shelf Water forming under ice shelf cavities. The vigour of these cascading flows during glacial / deglacial periods are currently not known.

### **6.3. Can glacial meltwater cause gully erosion?**

The pattern of gullying observed along the Ross Sea margin is consistent with ice grounding near to the shelf edge, as suggested by the occurrence of glacial facies in available sediment cores (Prothro et al., 2018; 2020). Deeply incised and V-shaped gullies are present at the Glomar Challenger Basin mouth, yet absent from the Pennell Trough mouth (Fig. 3; Fig. 8). The observation of a V-shaped, deeply incised and sinuous thalweg, suggests that the formation of gullies is dominated by fluid flow rather than generation by mechanisms such as slope failure which are likely to form escarpments and lack of well-defined thalweg (e.g. Kenyon, 1987; Simons and Senturk, 1992). Grounded ice can influence the availability of subglacial and ice front meltwater which can become sediment-laden and entrained into sediment-laden gravity flows down slope causing erosion of the seafloor (Anderson, 1999; Noormets et al., 2009; Ó Cofaigh et al., 2003). Subglacial meltwater is formed by processes such as geothermal heat fluxes, friction, strain heating and surface melting as shown by the presence of paleo-subglacial drainage systems such as subglacial lakes and meltwater channels on the continental shelf (e.g. Sugden et al., 1991; Simkins et al., 2017). Though surface melting is minimal in Antarctica at present day, it may be effective in certain areas and contribute to slope instabilities within glacier terminus systems (Rebesco et al, 2014).

At the mouth of Glomar Challenger Basin, gullies are greater in relief, length, width and sinuosity on the eastern side of the basin mouth, where upper slope gradients are  $\sim 3.5^\circ$  compared to smaller, straighter and higher density gullies to the west of the basin mouth where slope gradients increase to  $\sim 4.5^\circ$  (Fig. 3, 4). The small change in slope gradient across the continental slope likely reflects the proximity of the eastern part of the slope to the Eastern Ross Sea Trough Mouth Fan, which is characterised by outward bulging contours formed by margin progradation. The increase in slope gradient to the west is likely to cause higher velocities of down-slope flows, leading to greater flow confinement, narrow and straight gullies (Wynn et al., 2012). The differences in gully morphology may also reflect greater availability, or focussing, of sediment-laden subglacial meltwater to the east of Glomar Challenger Basin mouth, on the flank of the Eastern Ross Sea Fan (Rebesco et al., 1998; Noormets et al., 2009; Fig. 8). Meltwater may be drawn toward trough margins due to differences in subglacial water pressure gradients and additional frictional heat at trough margins caused by faster flowing ice streams, compared to slower moving ice on adjacent banks (Rothlisberger, 1972; Noormets et al., 2009; Boulton et al., 2007).

Meltwater can also form when intrusions of CDW reach the ice sheet front, causing rapid melting of marine terminating ice shelves and tidewater cliffs (Silvano et al., 2018). Sub-ice-shelf melt caused by intruding warm currents can cause energetic and turbulent plumes of very cold, fresh water to rise at the ice calving face due to reversed buoyancy differences (Jenkins et al., 2011; Truffer and Motyka, 2016). Similarly, buoyant plumes that track the underside of floating ice can also emerge from point-source meltwater channels under ice shelves (Carter and Fricker, 2012; Jenkins et al., 2011). Turbulent mixing drives convective motion at the ice-ocean interface which may cause sediment resuspension if the turbulence caused by the buoyancy effects of rising meltwater jets are great enough to resuspend recently deposited sediments at the shelf edge (Heese and Khodabaksh, 2006; Jenkins et al., 2011).

Where ice is grounded at the shelf edge, slope gradients may be great enough to allow sediment-laden gravity flows to evolve down slope. Both mechanisms of erosion by sediment-laden gravity flows can explain the pattern on deep gully incision at the Glomar Challenger Basin mouth, where ice grounded near to the shelf edge, and absence of gullies from the Pennell Trough, where ice grounded  $>120$  km from the shelf edge (Fig. 8; Fig. 9B).

#### **6.4. Can intruding warm currents erode the shelf edge?**



The region of greatest gully size and sinuosity (Fig. 3A, 4) occurs where numerical modelling studies show CDW intruding onto the shelf to the east of Glomar Challenger Basin (Morrison et al., 2020). Smaller and higher density gullies occur further west where CDW intrusions are reduced and dense shelf water cascading is greatest (Bergamasco et al., 2002; Morisson et al., 2020). Recent modelling shows a strong dynamic relationship between CDW and dense shelf water overflow within the Hillary Canyon with spatial distribution due to Coriolis driving dense shelf waters toward the west of the canyon (Morrison et al., 2020). As dense shelf water descends, less dense water is displaced within the canyon causing sea level height to decrease resulting in a barotropic pressure gradient that drives CDW shelfward (Morrison et al., 2020). Direct observations of CDW are absent at this location presently, however, simulated CDW velocities are shown to reach  $0.25 \text{ ms}^{-1}$  (Morrison et al., 2020). We suggest that intruding flows of CDW do not exert significant influence on gully morphology as comparisons with modelled and direct observations of cascading dense shelf water velocities reaching  $1 \text{ ms}^{-1}$  are shown to be too weak to incise glacial sediments at the shelf edge (Gordon et al., 2009; Morrison et al., 2020). The motion field in the areas surrounding CDW intrusions may allow recent fine-grained sediments to be resuspended and allow gully morphology to be maintained at the shelf edge, however are not strong enough to permit significant seafloor erosion here.

The spatial distribution and dynamic relationship between CDW intrusions and dense shelf water also acted during past glacial and interglacial periods, driven by Coriolis and the equilibrium between water mass density. When the ice sheet was grounded at the shelf edge, formation of dense shelf water over the continental shelf was likely reduced due to limited opportunity for sea ice formation, although dense water formation was likely to have continued seaward of the ice margin over the continental slope. It follows that dense shelf water cascading also occurred along the western flank of the Glomar Challenger Basin with intrusions of CDW likely across the eastern flank of the Glomar Challenger Basin. The incursion of CDW may have triggered the initial ice retreat and caused the release of a large amount of meltwater. This may explain the large size of the gullies compared to the western sector.

## **6.5. Paleo-gully formation**

New seismic data show paleo-gullies beneath gullies incising the modern seafloor (Fig. 3C), indicating that this region has been influenced by gully-forming processes over sustained periods of time. The surface gullies terminate above a strong parallel reflector, R1, that shoals toward the seafloor at the Pennell Trough, where both surface and paleo-gullies are absent. Reflector R1 is characterised by small (average relief of  $\sim 28 \text{ m}$  and width

of 0.24 km) gullies occurring in similar frequency across the shelf edge to gullies incising the modern seafloor. Gullies incising R1 do not follow the same spatial distributions to the surface gullies, with gullies located both directly beneath, and in regions absent of surface gullies (Fig. 3C). The small size of the gullies incising R1 compared to the modern seafloor implies formation by minimally erosive flows, or flows occurring over shorter time-scales before being abruptly filled (Shumaker et al., 2017). Reflector R1 may indicate a major climatic event such as major ice advance across the continental shelf; although, further evidence from sediment cores is required to constrain the age and magnitude of this transition further.

The paleo-gullies beneath R1 occur as both single gullies and in complexes in the same region as the surface gullies. Similarly to gullies incising R1, the paleo-gullies do not follow the same spatial distribution as gullies incising the modern seafloor, or those incising R1 (Fig. 3C). The size of the paleo-gullies beneath R1 are significantly greater in relief than the most recent seafloor-incising gullies indicating that gully-forming events were likely larger in the past or the processes that formed them were sustained over longer time periods, for example due to greater volumes of sediment and/or meltwater availability (Hayes et al., 1975). The size and stacked nature of the gullies implies that the shelf edge underwent periods of inactivity and partial infilling before gully incision restarted suggesting that a complex period of gully fill and erosion occurred (Shumaker et al., 2017). This suggests that gully activity was continuous over multiple glacial cycles and formed an important role in the development of the shelf edge and upper slope, with incision likely related to duration and persistence of ice-sheet residence.

The lack of gully spatial continuity with depth indicates that there is no preferential route or passage that processes, such as sediment laden subglacial meltwater released from beneath an ice sheet, or meltwater generated by warm intruding currents, follow on the continental slope. This suggests that ice sheet configuration varied at the shelf edge over multiple glacial cycles. As paleo-gullies are only observed at the mouth of the Glomar Challenger Basin, this may provide further evidence for sustained ice advance and retreat compared to a much more limited extent in the Pennell Trough.

## **6.6. How do gullies compare to other high-latitude continental margins?**

We put slope morphology observed at the Hillary Canyon head into global perspective to understand if cascading flows of dense shelf water exert consistent patterns of erosion on high-latitude continental margins. Analysis of gully morphometric parameters over ~2300 km of the Antarctic continental margin, including the western Antarctic Peninsula, Bellingshausen, Amundsen, Weddell and Ross seas show that gullies at the Glomar

Challenger Basin mouth are significantly different in morphology to gullies observed in other areas of dense shelf water cascading (Fig. 10). The Weddell Sea is a region of significant dense shelf water production, contributing to ~50% global Antarctic Bottom Water production (Budillon et al., 2011). Gullies at the Filchner Trough mouth, Weddell Sea, are smaller in relief, length and width, U-shaped in cross-section with low sinuosity and found on lower slope gradients ( $\sim 2.5^\circ$ ) (Gales et al., 2012). The significant difference in gully morphology between two globally important regions of dense shelf water cascading (Fig. 10), shows that these cascading flows do not exert consistent patterns of erosion on high-latitude continental margins under modern day conditions. It is likely that this pattern of erosion has greater dependence on other factors, such as glacier drainage basin size, regional oceanography, meltwater availability, glacial extent and polynya activity rather than the cascading flows themselves causing gully incision during interglacial conditions.

Analogous gullies to those observed at the Glomar Challenger Basin mouth form in regions unaffected by modern cascading flows of dense shelf water e.g. along the western Antarctic Peninsula margin and some Arctic margins e.g. Kongsfjorden Trough, Bear Island Trough and Adfjorden Trough (Noormets et al., 2009; Gales et al., 2013; Rui et al., 2019; Post et al., 2020). These gullies are characterised by V-shaped cross-sections, low gully lengths, medium sinuosities and similar reliefs and are found on medium slope gradients of  $\sim 6\text{-}9^\circ$  both within and outside cross-shelf trough confines (Gales et al., 2013). Due to the V-shaped and deeply incised morphologies, these gullies are suggested to form by processes dominated by suspended sediment load such as release of sediment-laden subglacial meltwater (e.g. Simons and Senturk, 1992). This is consistent with analysis of gullies observed along the Glomar Challenger Basin margin which suggest gullies formed by gravity flows generated by resuspension of sediment by glacial meltwater processes.

## 7. Conclusions

Shelf-slope processes and climatic variations can have significant influence on seafloor morphology, especially in Polar regions, where climate, ice sheet and sea level changes play a crucial role (Fig. 9). New geophysical and oceanographic data show that the Hillary Canyon is the main conduit for cascading flows of dense shelf water to the abyss with canyon levees likely formed of overbank deposits indicating a prolonged history of down-slope flows. Incisional gullies occur at the canyon head, which merge into channels and into the main canyon thalweg. The distribution of gullies along the shelf edge is not homogenous with a distinct absence of gullies in a region of intense modern dense shelf water export. The gullies correspond with maximum ice extent at the Ross Sea shelf edge indicating gully incision was likely controlled by glacial advance. At the Pennell Trough mouth,

gullies are absent as the maximum extent of grounded ice was >120 km inland of the shelf-edge. Glacial advance likely preconditioned the slope to down-slope processes such as release of sediment laden subglacial meltwater from the ice sheet terminus.

Our results suggest that cascading flows of dense shelf water are strong enough to prevent gully infilling and contribute to canyon-levee aggradation down-slope; however, do not contribute to significant gully incision at the shelf edge. During full-glacial conditions, where ice grounded at the shelf edge, the formation and cascading of dense shelf water was limited by lack of continental shelf polynya. Sediment laden subglacial meltwater released from beneath an ice sheet or meltwater generated by warm intruding currents that resuspends sediment may produce sediment gravity flows where slope gradients are great enough for flow ignition (e.g. ice front located at the shelf break). Understanding both modern and past processes influencing canyon morphology has important implications for reconstructing past ice sheet behaviour from sediment cores. Better definition of factors influencing seafloor morphology will assist future numerical modelling studies in predicting the dynamic behaviour of processes that influence changes to ice-shelf and sea level variations and applies to canyons around Antarctica more widely. These findings raise important questions concerning factors controlling ice advance, duration and persistence of ice-sheet residence at the shelf edge and what previously limited ice advance in Pennell Trough. Our findings show that gullies were absent in this region over multiple glacial cycles, perhaps indicating a stronger inflow of CDW here limited ice advance. The factors controlling the preferential locations of CDW intrusions are of utmost importance as major drivers of Antarctic ice sheet retreat.

Further sedimentological information is required to identify the timing and frequency of these slope processes and their reliance on climatic cycles more widely over previous millennia. This will help constrain links between paleo-ice sheet dynamics, paleo-oceanographic processes and slope processes which is crucial for understanding future changes.

## **8. Acknowledgements**

This work was supported by the EUROFLEETS Funding Program (ANTSSS project) and Italian National Antarctic Research Program (PNRA16 00205; ODYSSEA) projects. The authors thank Captain Franco Sedmak and crew of R/V OGS Explora; party chief Riccardo Codiglia; the technicians and scientific party of the expedition; We thank Laura de Steur for supplying the L-ADCP during the ANTSSS expedition and for processing of L-ADCP data. We acknowledge IHS Markit, Paradigm, Schlumberger for Kingdom and Vista

academic license to OGS. RM was funded by the Royal Society Te Apārangi Marsden Fund award MFP-VUW1808.

## 9. References

Alonso, B., Anderson, J.B., Diaz, J.T., Bartek, L.R. 1992. Pliocene-Pleistocene seismic stratigraphy of the Ross Sea: evidence of multiple ice sheet grounding episodes. In Contributions to Antarctic Research III, Antarctic Research Series 57, American Geophysical Union, Washington D.C, 93-103.

Anderson, J. 1999. Antarctic Marine Geology. Cambridge University Press.

Anderson, J., Bartek, L. 1990. Preliminary results of high-resolution seismic reflection survey of the Ross Sea continental shelf. Antarctic Journal of the US 25, 61-63.

Anderson, J., Conway, H., Bart, P., Witus, A., Greenwood, S., McKay, R., Hall, B., Ackert, R., Licht, K., Jakobsson, M., Stone, J. 2014. Ross Sea paleo-ice sheet drainage and deglacial history during and since the LGM. Quaternary Science Reviews 100, 31-54.

Anderson, J., Simkins, L., Bart, P., De Santis, L., Halberstadt, A., Olivo, E., Greenwood, S. 2019. Seismic and geomorphic records of Antarctic ice sheet evolution in the Ross Sea and controlling factors in its behaviour. Geological Society, London, Special Publications 475, 223-240.

Arndt, J., Schenke, H.W., Jakobsson, M., Nitsche, F.O., Buys, G., Goleby, B., Rebesco, M., Bohoyo, F., Hong, J.K., Black, J., Greku, R., Udintsev, G., Barrios, F., Reynoso-Peralta, W., Taisei, M., Wigley, R. 2013. The International Bathymetric Chart of the Southern Ocean (IBCSO) Version 1.0. PANGAEA, doi.org/10.1594/PANGAEA.805736.

Barker, P., Camerlenghi, A. 2002. Glacial history of the Antarctic Peninsula from Pacific margin sediments. Proceedings of the Ocean Drilling Program: Scientific Results 178, 1-40.

Bart, P.J., Anderson, J.B. 2000. Relative stability of the Antarctic ice sheets during the Plio-Pleistocene from the perspective of the continental shelf. Earth and Planetary Science Letters 182, 259–272.

Bart, P.J., Owolana, B. 2012. On the duration of West Antarctic Ice Sheet grounding events in Ross Sea during the Quaternary. Quaternary Science Reviews 47, 101-115.

569 Bensi, M., Kovacevic, V., Langone, L., Aliani, S., Ursella, L., Goszczko, I., Solwedel, T., Skogseth, R., Nilsen,  
 570 F., Deponte, D., Mansutti, P., Laterza, R., Rebesco, M., Rui, L., Lucchi, R.G., Wahlin, A., Viola, A.,  
 571 Beszczynska-Moller, A., Rubino, A. 2019. Deep flow variability offshore South-west Svalbard (Fram Strait).  
 572 *Water* 11, doi.org/10.3390/w11040683.

573 Bergamasco, A., Defendi, V., Zambianchi, E., Spezie, G. 2002. Evidence of dense water overflow on the Ross  
 574 Sea shelf-break. *Antarctic Science* 14, 271-277.

575 Boulton, G., Lunn, R., Vidstrand, P., Zatsepin, S. 2007. Subglacial drainage by groundwater-channel coupling,  
 576 and the origin of esker systems: Part 1 – glaciological observations. *Quaternary Science Reviews* 26, 1067-  
 577 1090.

578 Brancolini, G., Cooper, A., Coren, F. 1995. Seismic facies and glacial history in the western Ross Sea,  
 579 Antarctica. *Geology and Seismic Stratigraphy of the Antarctic Margin*, Antarctic Research Series 68, 209-233.

580 Budillon, G., Castagno, P., Aliani, S., Spezie, G., Padman, L. 2011. Thermohaline variability and Antarctic  
 581 bottom water formation at the Ross Sea shelf break. *Deep Sea Research Part I: Oceanographic Research Papers*  
 582 58, 1002-1018.

583 Canals, M., Puig, P., de Madron, X.D., Heussner, S., Palanques, A., Fabres, J. 2006. Flushing submarine  
 584 canyons. *Nature* 444, 354-357.

585 Carter, S.P., Fricker, H.A. 2012. The supply of subglacial meltwater to the grounding line of the Siple Coast,  
 586 West Antarctica. *Annals of Glaciology* 53, 267-280.

587 Clare, M., Hughes Clarke, J., Talling, P., Cartigny, M., Pratomo, D. 2016. Preconditioning and triggering of  
 588 offshore slope failures and turbidity currents revealed by most detailed monitoring yet at a fjord-head delta.  
 589 *Earth and Planetary Science Letters* 450, 208–220.

590 Colleoni, F., De Santis, L., Siddoway, S., Bergamasco, A., Golledge, N.R., Lohmann, G., Passchier, S., Siegert,  
 591 M.J. 2018. Spatio-temporal variability of processes across the Antarctic ice-bed-ocean interfaces. *Nature*  
 592 *Communications* 9, doi.org/10.1038/s41467-018-04583-0.

593 Cooper, A.K., Barrett, P.J., Hinz, K., Traube, V., Leitchenkov, G., Stagg, H.M.J. 1991. Cenozoic prograding  
594 sequences of the Antarctic continental margin: a record of glacio-eustatic and tectonic events. *Marine Geology*  
595 102, 175–213.

596 Damuth, J. 1978. Echo character of the Norwegian-Greenland Sea: Relationship to Quaternary sedimentation.  
597 *Marine Geology* 28, 1-36.

598 DeConto, R.M., Pollard, D., 2016. Contribution of Antarctica to past and future sea-level rise. *Nature* 531, 591–  
599 597.

600 De Santis, L., Anderson, J.B., Brancolini, G., Zayatz, I. 1995. Seismic record of late Oligocene through Miocene  
601 glaciation on the Central and Eastern Continental Shelf of the Ross Sea. In: Cooper, A.K., Barker, P.F.,  
602 Brancolini, G. (eds). *Geology and Seismic Stratigraphy of the Antarctic Margin*. Antarctic Research Series 68,  
603 AGU Washington, DC, 235-260.

604 Dinniman, M.S., Klinck, J.M., Smith Jr, W.O. 2003. Cross-shelf exchange in a model of the Ross Sea  
605 circulation and biogeochemistry. *Deep Sea Research Part II: Topical Studies in Oceanography* 50, 3103-3120.

606 Diviacco, P., Rebesco, M., Camerlenghi, A. 2006. Late Pliocene mega debris flow deposit and related fluid  
607 escapes identified on the Antarctic Peninsula continental margin by seismic reflection data analysis. *Marine*  
608 *Geophysical Researches* 27, 1-19.

609 Donda, F., O'Brien, P.E., De Santis, L., Rebesco, M., Brancolini, G., 2008. Mass wasting processes in the  
610 Western Wilkes Land margin: possible implications for East Antarctic glacial history. *Palaeogeography*,  
611 *Palaeoclimatology, Palaeoecology* 260, 77-91.

612 Dugan, B., Flemings, P. W. 2000. Overpressure and fluid flow in the New Jersey continental slope: Implications  
613 for slope failure and cold seeps. *Science* 289, 288-291.

614 Gales, J.A., Forwick, M., Laberg, J.S., Vorren, T.O., Larter, R.D., Graham, A.G.C., Baeten, N., Amundsen,  
615 H.B. 2013. Arctic and Antarctic submarine gullies – a comparison of high latitude continental margins.  
616 *Geomorphology* 201, 449-461.

617 Gales, J.A., Larter, R.D., Mitchell, N.C., Hillenbrand, C.-D., Østerhus, S., Shoosmith, D. 2012. Southern  
618 Weddell Sea shelf edge geomorphology: Implications for cold, high salinity water overflow as an Antarctic

619 gully-forming mechanism. *Journal of Geophysical Research – Earth Surface* 117, F0421,  
620 doi.org/10.1029/2012JF002357.

621 Gales, J., Zgur, F., Accettella, D., Bergamasco, A., Codiglia, R., Colleoni, F., Cuffaro, M., DeSantis, L.,  
622 DiCurzio, E., Filippone, P., Gordini, E., Kim, S., Lopez, C., Kovacevic, V., Mansutti, P., Olivo, E., Rebesco,  
623 M., Sterzai, P., Tomini, I., Visnovic, G., Yanguang, L. 2017. Antarctic Ice Sheet Stability from continental  
624 slope processes investigation (ANTSSS). EUROFLEETS2 Cruise Summary Report, pp 61.

625 Galy, V., France-Lanord, C., Beyssac, O., Faure, P., Kudrass, H., Palhol, F. 2007. Efficient organic carbon  
626 burial in the Bengal fan sustained by the Himalayan erosional system. *Nature* 450, 407–410.

627 Golledge, N.R., Levy, R.H. 2011. Geometry and dynamics of an East Antarctic Ice Sheet outlet glacier, under  
628 past and present climates. *Journal of Geophysical Research - Earth Surface* 116, F3,  
629 doi.org/10.1029/2011JF002028.

630 Gordon, A.L., Orsi, A.H., Muench, R., Huber, B.A., Zambianchi, E., Visbeck, M. 2009. Western Ross Sea  
631 continental slope gravity currents. *Deep-Sea Research II* 56, 796-817.

632 Hage, S., Cartigny M.J.B., Sumner, E.J., Clare, M.A., Hughes Clarke, J.E., Talling, P.J., Lintern, D.G.,  
633 Simmons, S.M., Silva Jacinto, R., Vellinga, A.J., Allin, J.R., Azpiroz-Zabala, M., Gales, J.A., Hizzett, J., Hunt,  
634 J., Mozzato, A., Partson, D., Pope, E., Stacey, C., Symons, W., Vardy, M., Watts, C. 2019. Direct monitoring  
635 reveals initiation of turbidity currents from extremely dilute river plumes. *Geophysical Research Letters*,  
636 doi.org/10.1029/2019GL084526.

637 Halberstadt, A.R., Simkins, L.M., Greenwood, S.L., Anderson, J.B. 2016. Past ice sheet behavior: retreat  
638 scenarios and changing controls in the Ross Sea, Antarctica. *The Cryosphere* 10, 1003–1020.

639 Hayes, D.E., Frakes, L.A. 1975. General synthesis: Deep Sea Drilling Project 28. In: Hayes D.E., Frakes L.A. et  
640 al. (eds). *Initial Reports of the Deep Sea Drilling Project*. US Government Printing Office, Washington, DC 28,  
641 919–942.

642 Heese, R., Khodabakhsh, S. 2006. Significance of fine-grained sediment lofting from meltwater generated  
643 turbidity currents for the timing of glaciomarine sediment transport into the deep sea. *Sedimentary Geology* 186,  
644 1-11.



645 IPCC. 2019. Summary for Policymakers. In: IPCC Special Report on the Ocean and Cryosphere in a Changing  
 646 Climate. Pörtner, H.-O., Roberts, D.C., Masson-Delmotte, V., Zhai, P., Tignor, M., Poloczanska, E.,  
 647 Mintenbeck, K., Nicolai, M., Okem, A., Petzold, J., Rama, B., Weyer, N. (eds). In press.

648 Jacobs, S.S. 2004. Bottom water production and its links with the thermohaline circulation. *Antarctic Science*  
 649 16, 427-437.

650 Jacobs, S.S., Fairbanks, R.G., Horibe, Y. 1985. Origin and evolution of water masses near the Antarctic  
 651 continental margin: evidence from  $H_2^{18}O_2/H_2^{16}O_2$  ratios in seawater. *Antarctic Research Series* 43, 59–85.  
 652

653 Jacobs, S.S., Giulivi, C.F., Mele, P.A. 2002. Freshening of the Ross Sea during the late 20th Century. *Science*  
 654 297, 386–389.

655  
 656 Jacobs, W., Le Hir, P., Van Kesteren, W., Can, P. 2011. Erosion threshold for sand-mud mixtures, *Continental*  
 657 *Shelf Research* 31, S14– S2.

658 Jaeger, J.M., Nittrouer, C.A., Demaster, D.J., Kelchner, C., Dunbar, R.B. 1996. Lateral transport of settling  
 659 particles in the Ross Sea and implications for the fate of biogenic material. *Journal of Geophysical Research*  
 660 101, 18479–18488.

661 Jenkins, A. 2011. Convection driven melting near the grounding lines of ice shelves and tidewater glaciers.  
 662 *Journal of Physical Oceanography* 41, doi.org/10.1175/JPO-D-11-03.1.

663 Joughin, I., Alley, R. B. 2011. Stability of the West Antarctic ice sheet in a warming world. *Nature Geoscience*,  
 664 4, 506-513.

665 Kenyon, N.H. 1987. Mass-wasting features on the continental slope of northwest Europe. *Marine Geology* 74,  
 666 57-77.

667 Laberg, J.S., Vorren, T.O. 1995. Late Weichselian submarine debris flows deposits on the Bear Island Trough  
 668 Mouth Fan. *Marine Geology* 127, 45  
 669

670 Laberg, J.S., Vorren, T.O. 2000. Flow behaviour of the submarine glacigenic debris flows on the Bear Island  
 671 trough mouth fan, western Barents Sea. *Sedimentology* 47, 1105-1117.

672 Lee, J.R., Philips, E. 2013. Glacitectonics – a key approach to examining ice dynamics, substrate rheology and  
 673 ice-bed coupling. *Proceedings of the Geologists' Association* 124, 731-737.

674 Long, D., Stevenson, A., Wilson, C., Bulat, J. 2003. Slope failures in the Faroe-Shetland channel. In: Locat, J.,  
 675 Mienert, J. (eds). *Submarine Mass Movements and Their Consequences*. Kluwer Academic, The Netherlands.

676 Lucchi, R., Rebesco, M., Camerlenghi A., Buseti, M., Tomadin, L., Villa, G., Persico, D., Morigi, C., Bonci,  
 677 M., Giorgetti, G. 2002. Mid-late Pleistocene glacial-marine sedimentary processes of a high-latitude, deep sea  
 678 sediment drift (Antarctic Peninsula Pacific margin). *Marine Geology* 189, 343-370.

679 Maier, K.L., Rosenberger, K., Paull, C.K., Gwiazda, R., Gales, J., Lorenson, T., Barry, J., Talling, P.J.,  
 680 McGann, M., Xu, J.P., Lundsten, E., Anderson, K., Litvin, S.Y., Parsons, D., Clare, M.A., Simmons, S.M.,  
 681 Sumner, E.J., Cartigny, M.J., and the Monterey Coordinated Canyon Experiment Team. 2019. Sediment and  
 682 organic carbon transport and deposition driven by internal tides along Monterey Canyon, offshore  
 683 California. *Deep-Sea Research I*, doi.org/10.1016/j.dsr.2019.103108.

684 Manabe, S., Stouffer, R.J. 1995. Simulation of abrupt climate change induced by freshwater input to the North  
 685 Atlantic Ocean. *Nature* 378, 165-167.

686 Maslin, M., Owen, M., Day, S., Long, D. 2004. Linking continental-slope failures and climate change: Testing  
 687 the clathrate gun hypothesis. *Geology* 32, 53-56.

688 McCave, I.N. 1984. Erosion, transport and deposition of fine-grained marine sediments. *Geological Society*  
 689 *London Special Publication* 15, 35– 69.

690 McKay, R., Golledge, N., Maas, S., Naish, T., Levy, R., Dunbar, G., Kuhn, G. 2016. Antarctic marine ice-sheet  
 691 retreat in the Ross Sea during the early Holocene. *Geology* 44, 7-10.

692 McKay, R., De Santis, L., Kulhanek, D., and the Expedition 374 Scientists. 2019. *Proceedings of the*  
 693 *International Ocean Discovery Program Volume 374*. Publications.iodp.org,  
 694 doi.org/10.14379/iodp.374.107.2019.

695 Melles, M., Kuhn, G. 1993. Sub-bottom profiling and sedimentological studies in the southern Weddell Sea,  
 696 Antarctica: evidence for large scale erosional / depositional processes. *Deep-Sea Research* 40, 739-760.

697 Morrison, A., Hogg, A., England, M., Spence, P. 2020. Warm circumpolar deep water transport toward  
698 Antarctica driven by local dense water exports in canyons. *Science Advances* 6, eaav2516.

699 Nettles, M., Ekström, G. 2010. Glacial earthquakes in Greenland and Antarctica. *Annual Review of Earth and*  
700 *Planetary Sciences* 38, 467-491.

701 Nilsen, T.H., Shew, R.D., Steffens, G.S., Studlick, J.R.J. 2008. Atlas of Deep-water Outcrops. AAPG Studies in  
702 *Geology* 56, 504 pp.

703 Noormets, R., Dowdeswell, J., Larter, R., Ó Cofaigh, C., Evans, J. 2009. Morphology of the upper continental  
704 slope in the Bellingshausen and Amundsen seas – implications for sedimentary processes at the shelf edge of  
705 West Antarctica. *Marine Geology* 258, 100-114.

706 Normandeau, A., Dietrich, P., Hughes Clarke, J.E., Van Wychen, W., Lajeunesse, P., Burgess, D., Ghienne, J.F.  
707 2019. Retreat pattern of glaciers controls the occurrence of turbidity currents on high-latitude fjord deltas  
708 (eastern Baffin Island). *Journal of Geophysical Research - Earth Surface* 124, doi.org/10.1029/2018JF004970.

709 Ó Cofaigh, C., Taylor, J., Dowdeswell, J., Pudsey, C. 2003. Palaeo-ice streams, trough mouth fans and high-  
710 latitude continental slope sedimentation. *Boreas* 32, 37-55.

711 Orsi, A.H., Wiederwohl, C.L. 2009. A recount of Ross Sea waters. *Deep Sea Research, Part II. Topical Studies*  
712 *in Oceanography* 56, 778–795.

713 Padman, L., Siegfried, M., Fricker, H. 2018. Ocean tide influences on the Antarctic and Greenland Ice Sheets.  
714 *Review of Geophysics* 56, 142-184.

715 Palanques, A., Puig, P., Latasa, M., Scharek, R. 2009. Deep sediment transport induced by storms and dense  
716 shelf-water cascading in the northwestern Mediterranean basin. *Deep Sea Research Part I: Oceanographic*  
717 *Research Papers* 56, 425-434.

718 Pattyn, F., Van Huele, W. 1998. Power Law or Power Flaw. *Earth Surface Processes and Landforms* 23, 761-  
719 767.

720 Petrelli, P., Bindoff, N., Bergamasco, A. 2008. The sea ice dynamics of Terra Nova Bay and Ross Ice Shelf  
721 polynyas during a spring and winter simulation. *Journal of Geophysical Research* 113, C09003,  
722 doi:10.1029/2006JC004048.

723 Petrini, M., Colleoni, F., Kirchner, N., Hughes, A.L.C., Camerlenghi, A., Rebesco, M., Lucchi, R.G., Forte, E.,  
 724 Colucci, R.R., Noormets, R. 2018. Interplay of grounding-line dynamics and sub-shelf melting during retreat of  
 725 the Bjornoyrenna Ice Stream. *Scientific Reports* 8, DOI:10.1038/s41598-018-25664-6.

726 Pike, L., Gaskin, S., Ashmore, P. 2018. Flume tests of fluvial erosion mechanisms in till-bed channels. *Earth*  
 727 *Surface Processes and Landforms* 43, 259-270.

728 Piper, D., Cochonat, P., Morrison, M. 1999. Sidescan sonar evidence for progressive evolution of submarine  
 729 failure into a turbidity current: the 1929 Grand Banks event. *Sedimentology* 46, 79-97.

730 Pope, E., Normandeau, A., Ó Cofaigh, C., Stokes, C., Talling, P. 2019. Controls on the formation of turbidity  
 731 current channels associated with marine-terminating glaciers and ice sheets. *Marine Geology* 415, 105951.

732 Post, A., O'Brien, P., Edwards, S., Carroll, A., Malakoff, K., Armand, L. 2020. Upper slope processes and  
 733 seafloor ecosystems on the Sabrina continental slope, East Antarctica. *Marine Geology* 422, 106091.

734 Prothro, L., Majewski, W., Yokoyama, Y., Simkins, L., Anderson, J., Yamane, M., Miyairi, Y., Ohnkouchi, N.  
 735 2020. Timing and pathways of East Antarctic Ice Sheet retreat. *Quaternary Science Reviews* 230, 106166.

736 Prothro, L., Simkins, L., Majewski, W., Anderson, J. 2018. Glacial retreat patterns and processes determined  
 737 from integrated sedimentology and geomorphology records. *Marine Geology* 395, 104-119.

738 Purkey, S., Johnson, G. 2010. Warming of global abyssal and deep Southern Ocean waters between the 1990s  
 739 and 2000s: contributions to global heat and sea level rise budgets. *Journal of Climate* 23, 6336-6351.

740 Rahmstorf, S. 1994. Rapid climate transitions in a coupled ocean-atmosphere model. *Nature* 372, 82-85.

741 Rebesco, M., Camerlenghi, A. 2008. Late Pliocene margin development and mega debris flow deposits on the  
 742 Antarctic continental margins: Evidence of the onset of the modern Antarctic Ice Sheet? *Palaeogeography,*  
 743 *Palaeoclimatology, Palaeoecology* 260, 149-167.

744 Rebesco, M., Camerlenghi, A., Volpi, V., Neagu, C., Accettella, D., Lindberg, B., Cova, A., Zgur, F., Magico  
 745 Party. 2007. Interaction of processes and importance of contourites: insights from the detailed morphology of  
 746 sediment Drift 7, Antarctica. *Geological Society, London, Special Publications* 276, 95-110.

747 Rebesco, M., Hernandez-Molina, J., Van Rooij, D., Wahlin, A. 2014. Contourites and associated sediments  
 748 controlled by deep-water circulation processes: State of the art and future considerations. *Marine Geology* 352,  
 749 111-154.

750 Rebesco, M., Camerlenghi, A., Zanolla, C. 1998. Bathymetry and morphogenesis of the continental margin west  
 751 of the Antarctic Peninsula. *Terra Antarctica* 4, 715-725.

752 Rebesco, M., Larter, R., Camerlenghi, A., Barker, P. 1996. Giant sediment drifts on the continental rise west of  
 753 the Antarctic Peninsula. *Geo-Marine Letters* 16, 65-75.

754 Rignot, E., Mouginot, J., Scheuchl, B., Van den Broeke, M., van Wessem, M.J., Morlighem, M. 2019. Four  
 755 decades of Antarctic Ice Sheet mass balance from 1979-2017. *Proceedings of the National Academy of*  
 756 *Sciences*, doi.org/10.1073/pnas.1812883116.

757 Robertson, R., Beckmann, A., Hellmer, H. 2003. M2 tidal dynamics in the Ross Sea. *Antarctic Science* 15, 41–  
 758 46.

759 Rothlisberger, H. 1972. Water pressure in intra- and subglacial channels. *Journal of Glaciology* 11, 177-203.

760 Rui, L., Rebesco, M., Casamor, J.L., Laberg, J.S., Rydningen, T.A., Caburlotto, A., Forwick, M., Urgeles, R.,  
 761 Accettella, D., Lucchi, R.G., Barsanti, M., Demarte, M., Ivaldi, R., Delbono, I. 2019. Geomorphology and  
 762 development of a high-latitude channel system: the INBIS channel case (NW Barents Sea, Arctic). *Arktos* 5, 15-  
 763 29.

764 Shumaker, L.E., Jobe, Z.R., Graham, S.A. 2017. Evolution of submarine gullies on a prograding slope: Insights  
 765 from 3D seismic reflection data. *Marine Geology* 393, 35-46.

766 Seidov, D., Barron, E.J., Haupt, B.J. 2001. Meltwater and the global ocean conveyor: northern versus southern  
 767 connections. *Global and Planetary Change* 30, 253–266.

768 Seidov, D., Stouffer, R., Haupt, B. 2005. Is there a simple bi-polar ocean seesaw? *Global and Planetary change*  
 769 49, 19-27.

770 Shipp, S., Anderson, J.B., Domack, E.W. 1999. Late Pleistocene / Holocene retreat of the west Antarctic ice-  
 771 sheet system in the Ross Sea. Part 1. Geophysical results. *Geological Society of America Bulletin* 111, 1486-  
 772 1516.

773 Silvano, A., Rintoul, S.R., Pena-Molina, B., Hobb, W.R., Van Wijk, E., Aoki, S., Tamura, T., Williams, G.D.  
 774 2018. Freshening by glacial meltwater enhances melting of ice shelves and reduces formation of Antarctic  
 775 bottom water. *Science Advances* 4, doi.org/10.1126/sciadv.aap9467.

776 Simkins, L., Anderson, J., Greenwood, S., Gonnermann, H., Prothro, L., Halberstadt, A., Stearns, L., Pollard,  
 777 D., De Conto, R. 2017. Anatomy of a meltwater drainage system beneath the ancestral East Antarctic ice sheet.  
 778 *Nature Geoscience* 10, 691-697.

779 Simons, D.B., Sentürk, F. 1992. *Sediment Transport Technology: Water and Sediment Dynamics*. Water  
 780 Resources Publications, Highlands Ranch, Colorado, 901 pp.

781 Smith Jr, W., Nelson, D., DiTullio, G., Leventer, A. 1996. Temporal and spatial patterns in the Ross Sea:  
 782 Phytoplankton biomass, elemental composition, productivity and growth rates. *Journal of Geophysical*  
 783 *Research: Oceans* 101, 18455-18465.

784 Sugden, D.E., Denton, D.H., Marchant, D.R. 1991. Subglacial meltwater channel system and ice sheet over  
 785 riding of the Asgard range, Antarctica. *Geografiska Annaler* 73A, 109-121.

786 Talling P. 2014. On the triggers, resulting flow types and frequency of subaqueous sediment density flows in  
 787 different settings. *Marine Geology* 352, 155–182.

788 Traube, V., Zayatz, I. 1993. Main stages of development of the Eastern Basin, Ross Sea, imprinted in its  
 789 structure. In *LIRA workshop on Landscape Evolution – a multidisciplinary approach to the relation of Cenozoic*  
 790 *climate change and tectonics in the Ross Sea area, Antarctica*. Wateren, F., van der Verbers, A., Tessensohl, F.  
 791 (eds). *Rijks Geol Dienst, Haarlem, Netherlands*, pp. 91-94.

792 Truffer, M., Motyka, R.J. 2016. Where glaciers meet water: subaqueous melt and its relevance to glaciers in  
 793 various settings. *Review of Geophysics* 54, doi.org/10.1002/2015RG000494.

794 Vanneste, L., Larter, R. 1995. Deep-tow boomer survey of the Antarctic Peninsula Pacific margin: an  
 795 investigation of the morphology and acoustic characteristics of late Quaternary sedimentary deposits on the  
 796 outer continental shelf and upper slope. In: Cooper, A., Barker, B., Brancolini, B. (eds). *Geology and seismic*  
 797 *stratigraphy of the Antarctic margin*. Antarctic Research Series 68, American Geophysical Union, Washington,  
 798 D.C., 97-121.

Volpi, V., Camerlenghi, A., Hillenbrand, C.-D., Rebesco, M., Ivaldi, R. 2003. Effects of biogenic silica on sediment compaction and slope stability on the Pacific margin of the Antarctic Peninsula. *Basin Research* 15, 339–363.

Vorren, T.O., Laberg, J.S., Blaume, F., Dowdeswell, J.A., Kenyon, N.H., Mienert, J., Rumohr, J., Werner, F. 1998. The Norwegian-Greenland Sea continental margins: Morphology and late Quaternary sedimentary processes and environment. *Quaternary Science Reviews* 17, 273-302.

Weaver, A., Saenko, O., Clark, P., Mitrovica, J. 2003. Meltwater Pulse 1A from Antarctica as a trigger of the Bolling-Allerod Warm Interval. *Science* 299, 1709-1713.

Wynn, R., Talling, P., Masson, D., Le Bas, T., Cronin, B., Stevenson, C. 2012. The influence of subtle gradient changes on deep-water gravity flows: a case study from the Moroccan turbidite system. In: Prather, B.E; Deptuck, M.E; Mohrig, D; Van Hoorn, B; Wynn, R.B, (eds.). *Application of the Principles of Seismic Geomorphology to Continental-Slope and Base-of-Slope Systems: Case Studies from Seafloor and Near Seafloor Analogues: SEPM, Special Publication 99*, 371-383.

Zachos, J., Pagani, M., Sloan, L., Thomas, E., Billups, K. 2001. Trends, rhythms and aberrations in global climate 65 Ma to present. *Science* 292, 686-693.

## 10. Figure captions

Figure 1. A. Study area in the Ross Sea. White box shows location of (B). Bathymetric data is International Bathymetric Chart of the Southern Ocean (IBSCO, Arndt et al., 2013). Yellow triangle is position of cores RS14-BC3 and RS14-C3. Contour spacing is 200 m. B. Hillary Canyon regional bathymetry taken from IBSCO. White lines indicate positions of along and down-slope profiles shown in (C). White boxes show locations of Fig. 2, 3 and 5. Yellow triangle is position of cores RS14-BC3 and RS14-C3. C. Along and down-slope profiles across the Hillary Canyon derived from bathymetry using IBSCO. Stars highlight position of along-slope profiles shown in (B).

Figure 2. Submarine slide morphology and prograded continental margin at the mouth of the Glomar Challenger Basin. A. Slide morphology. Hillshaded bathymetry is gridded at 50 m. Regional bathymetry is from IBSCO.

827 Contour spacing is 50 m. Black lines mark location of single channel seismic lines IT17RS305 and IT17RS306.  
828 B. Seismic line IT17RS306 (near trace). C. Interpretation of seismic line IT17RS306 (near trace).

829 Figure 3. A. Morphology at the head of the Hillary Canyon, Ross Sea. Hillshaded bathymetry gridded at 50 m  
830 cell size. Contour spacing is 50 m. Background bathymetric data is International Bathymetric Chart of the  
831 Southern Ocean (IBSCO). Black lines mark location of single channel seismic lines IT17RS305 in (B) and  
832 IT17RS306. Black dashed line x-x' locates along-slope profile in (A). White dashed lines b-b' and c-c' locate  
833 sub-bottom profiles in (D) and (E). B. Single channel seismic line IT17RS305. Black box locates (C). C. Zoom-  
834 in of seismic line IT17RS305 located in (B). D. Unmigrated sub-bottom profile located in (A). E. Unmigrated  
835 sub-bottom profile located in (A).

836 Figure 4. Gully morphometric parameters along profile X-X' located in Figure 3A. Width of bars in top two  
837 panels correspond to gully width. Black diamonds correspond to average slope gradient ( $^{\circ}$ ) of the upper slope  
838 with distance parallel to the shelf edge.

839 Figure 5. A. Morphology of the Hillary Canyon thalweg. Hillshaded bathymetry is gridded at 50 m. Contour  
840 spacing is 50 m. Location of (A) shown in Figure 1B. B. Single channel seismic line IT17RS303 showing cross-  
841 section through the Hillary Canyon thalweg and canyon levees.

842 Figure 6. Oceanographic measurements along profile a-a'. A. Temperature data from 20 eXpendable  
843 BathyThermograph (XBT) profiles along profile a-a' located in (C). B. Current velocity data from Acoustic  
844 Doppler Current Profiler along profile a-a' located in (C). C. Hillshaded bathymetric data gridded at 50 m at the  
845 head of the Hillary Canyon, Ross Sea. Black line locates profile a-a' shown in (A) and (B). Blue lines are  
846 current vectors indicating current direction at 400 m water depth along dashed line in (B). Red stars locate eight  
847 Conductivity Temperature Depth profiles shown in Fig. 7A.

848 Figure 7. Oceanographic measurements at the head of the Hillary Canyon, Ross Sea. A. Conductivity  
849 Temperature Depth (CTD) profiles with fluorescence and turbidity sensor data. Location of CTD profiles are  
850 shown in Fig. 6C. B. Lowered-Acoustic Doppler Current Profiler data. Positions are shown in Fig. 6C. Red  
851 dashed line marks 0.7 m/s for comparison in all profiles.

852 Figure 8. Inferred ice position at Last Glacial Maximum. Background bathymetric data is International  
853 Bathymetric Chart of the Southern Ocean (IBSCO). Contour spacing is 50 m. Hillshaded bathymetry from  
854 ANTSSS expedition gridded at 50 m cell size. White dashed line is inferred ice extent at LGM taken from



Halberstadt et al. (2016). GZW is Grounding Zone Wedge position taken from Halberstadt et al. (2016). MR is morainal ridge. Red lines are gully positions.

Figure 9. Schematic of canyon head processes operating in glacial vs interglacial settings. A. Interglacial / modern conditions where gravity flows are generated fine grained biogenic / hemipelagic material that is resuspended by energetic cascading cold, dense water. B. Glacial conditions where energetic turbidity currents may be generated by either: the release of subglacial meltwater; meltwater generated by intruding warm currents at the ice front; slope failure. HSSW is High Salinity Shelf Water.

Figure 10. Antarctic gully morphometric parameters. A. Gully length vs gully relief. B. Gully width vs gully length. C. Gully sinuosity vs cross sectional shape. Data from the Weddell Sea, Bellingshausen Sea, Amundsen Sea, Western Antarctic Peninsula (WAP) taken from Gales et al. (2013). Ross Sea data from this study. For calculations of gully parameters, see SM.Fig.1.

## 11. Supplementary Material

SM Table 1. Variables used in calculations [1]

Value	Description	Data source
$u$	Depth averaged flow speed ( $\text{m/s}^{-1}$ )	This study; $1 \text{ m/s}^{-1}$
$C_d$	Friction factor	<i>Dimensionless (typically 0.0025)</i>
$P$	Water density	<i>This study; 1028.27 (cold water density)</i>

SM Figure 1. Measured gully morphometric parameters. A. Cross sectional view of gully where  $G^w$  is gully width (distance between points of maximum curvature of gully flanks);  $G^l$  is gully relief (vertical distance from maximum gully incision to line defining gully width); and  $G^{st}$  is gully steepness (ratio between gully relief and width). B. Plan view of gully thalweg where  $G^L$  is gully length,  $G^{SL}$  is straight light distance of gully length and  $G^s$  is gully sinuosity (ratio of gully length vs straight-line distance of gully length; where 1 = straight and  $>1$  indicates increasing sinuosity).

SM Figure 2. Cumulative grain size data for cores RS14-BC3 and RS13-C3 (locations marked in Fig 1). A. Cumulative grain size plot for box core RS14-BC3 (0-5 cm core depth). B. Cumulative grain size plot for core RS14-C3 (0-25 cm core depth). Depth of samples chosen to represent interglacial sediments. Outlier sample 24-

879 25 highlighted in key. C. Grain size volume measurements of sand-silt-clay, sand ( $63\ \mu\text{m}$  -  $2\ \text{mm}$ ), silt ( $2\ \mu\text{m}$  -  
880  $63\ \mu\text{m}$ ) and clay ( $< 2\ \mu\text{m}$ ) for gravity core RS14-C3. D. Grain size volume measurements of sand-silt-clay,  
881 where sand ( $63\ \mu\text{m}$  -  $2\ \text{mm}$ ), silt ( $2\ \mu\text{m}$  -  $63\ \mu\text{m}$ ) and clay ( $< 2\ \mu\text{m}$ ) for box core RS14-BC3. Gravel counts ( $>$   
882  $2\text{mm}$ ) shown in right column.

883

884

885

886

887

888

889

890

891

892

893

894

895

896

897

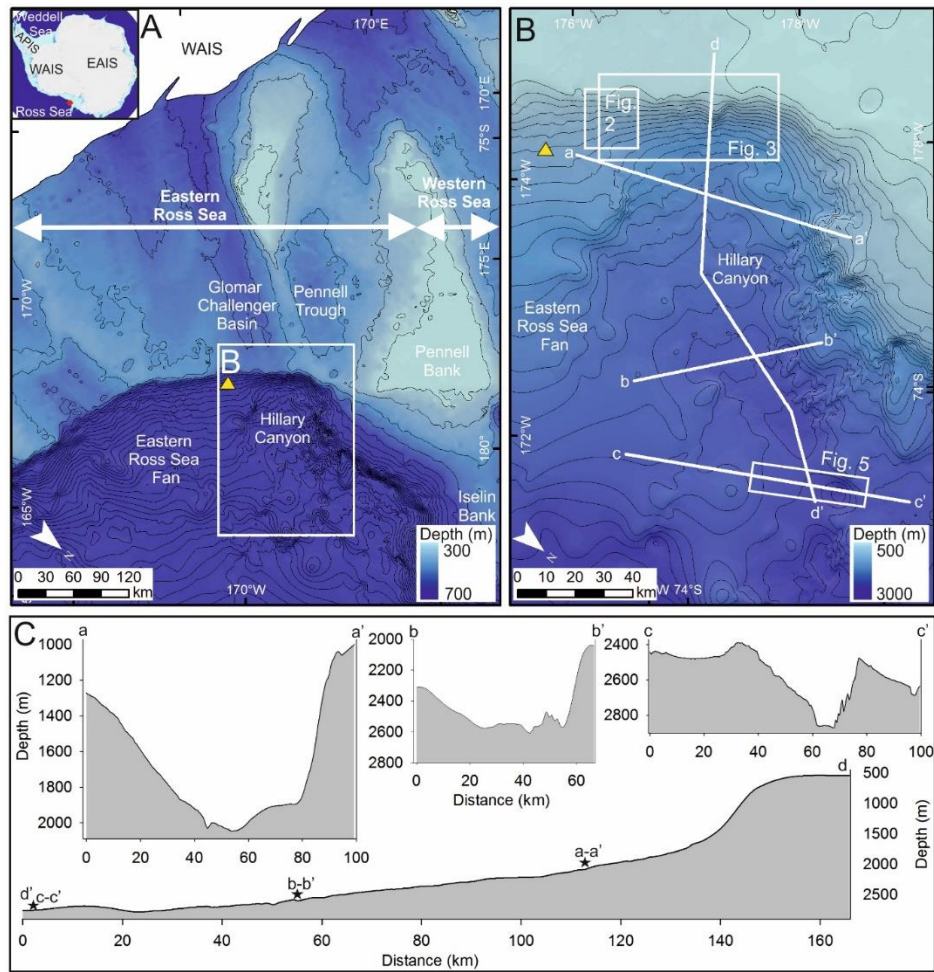
898

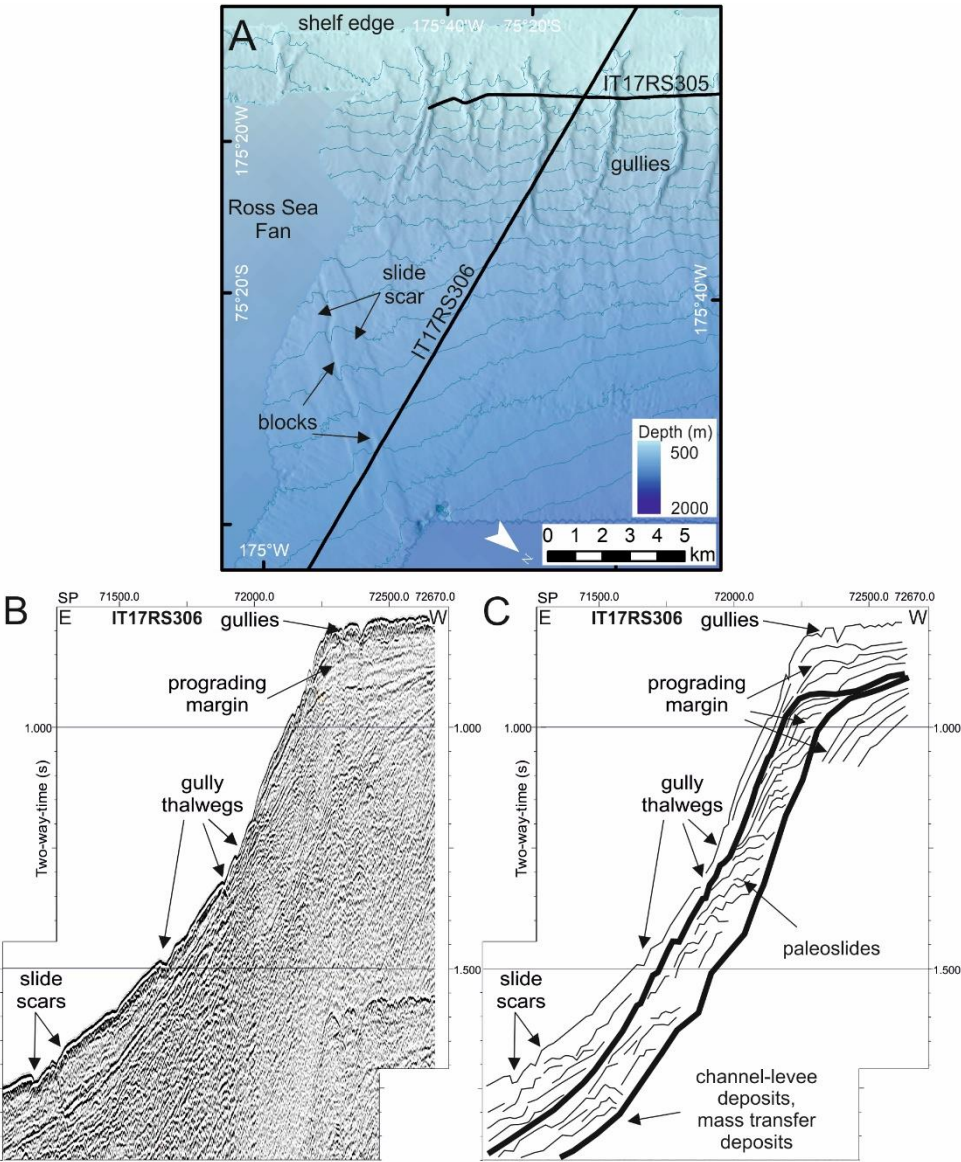
899

900

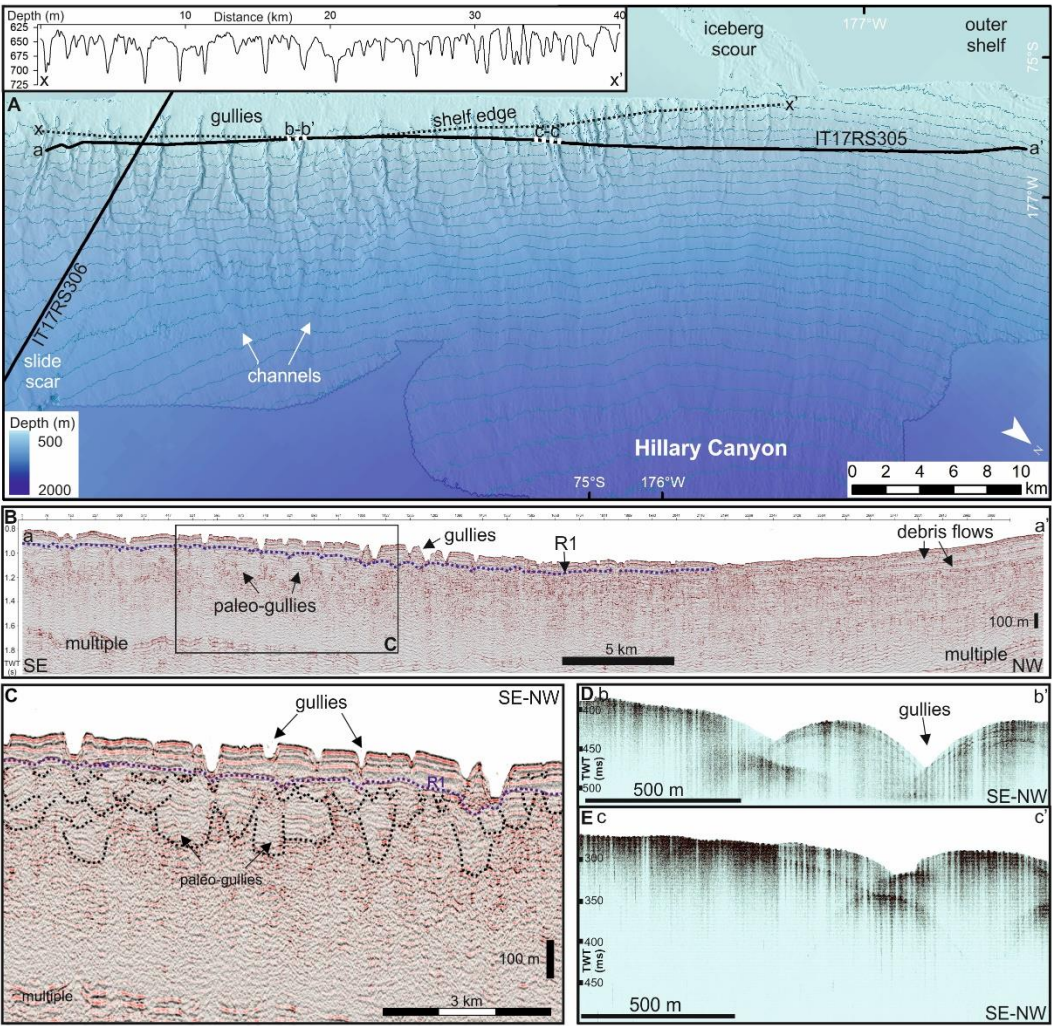
## 12. Figures

Figure 1.



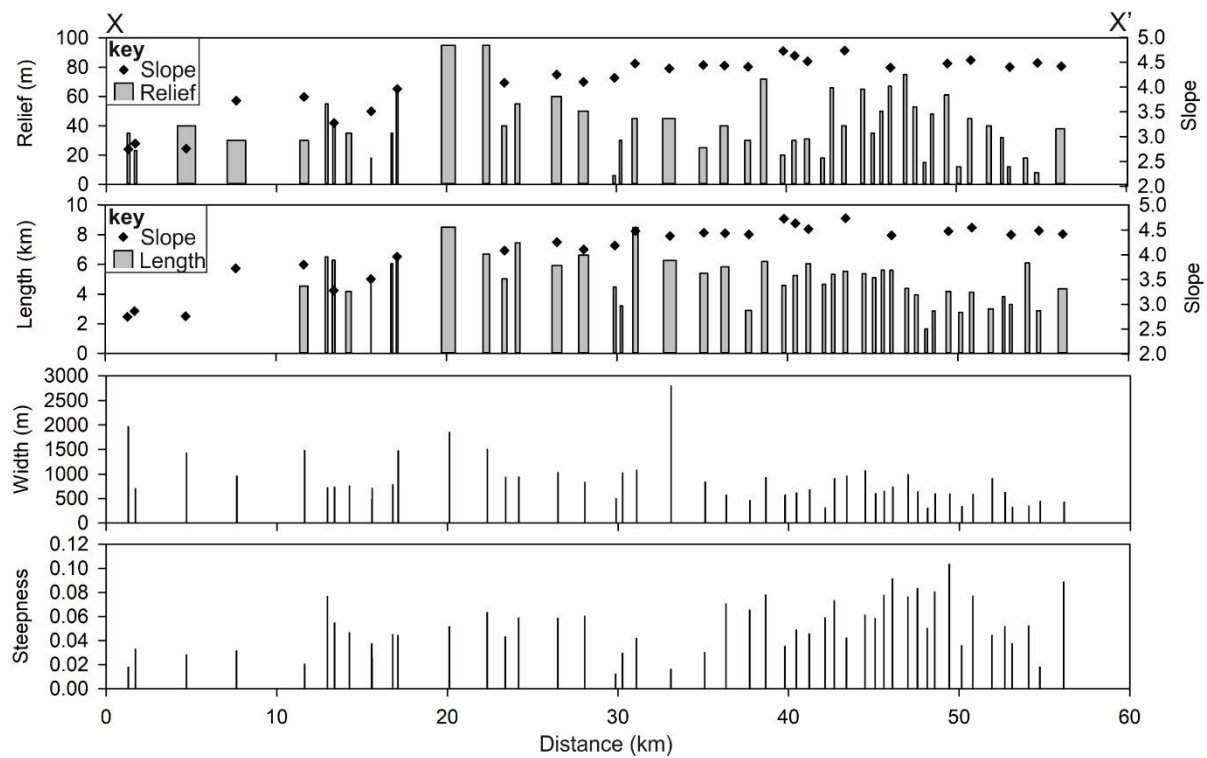


920 Figure 3





930 Figure 4



931

932

933

934

935

936

937

938

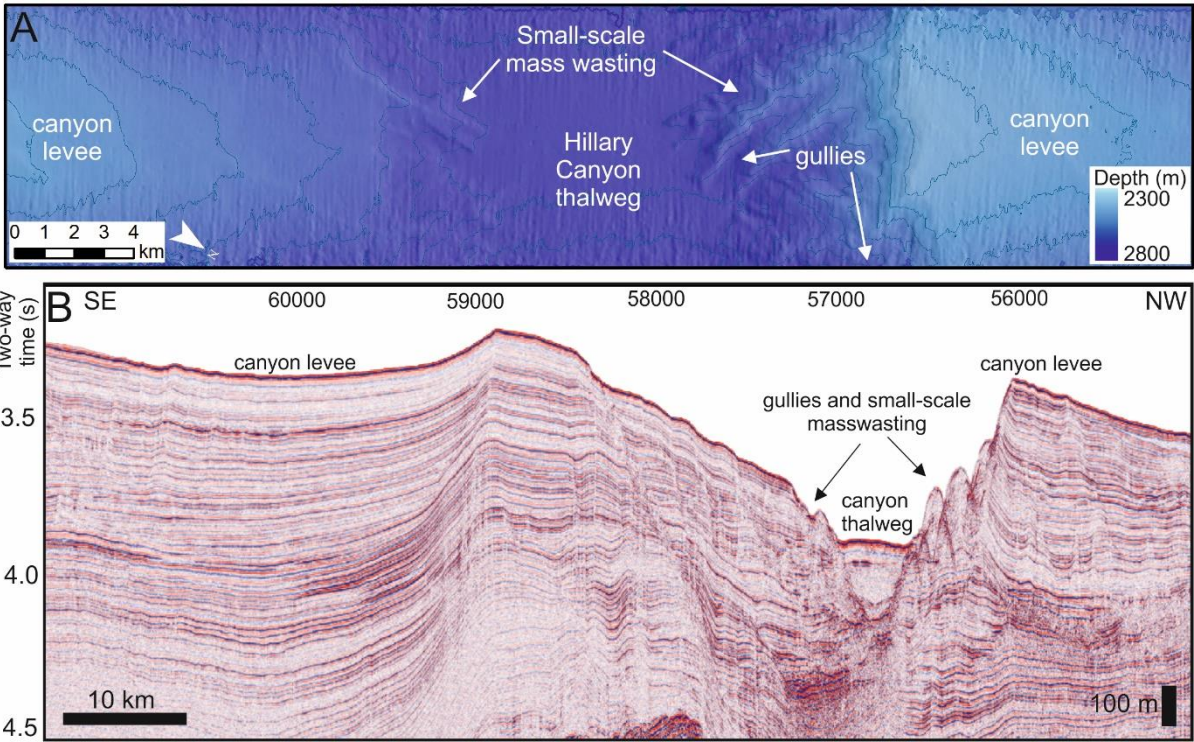
939

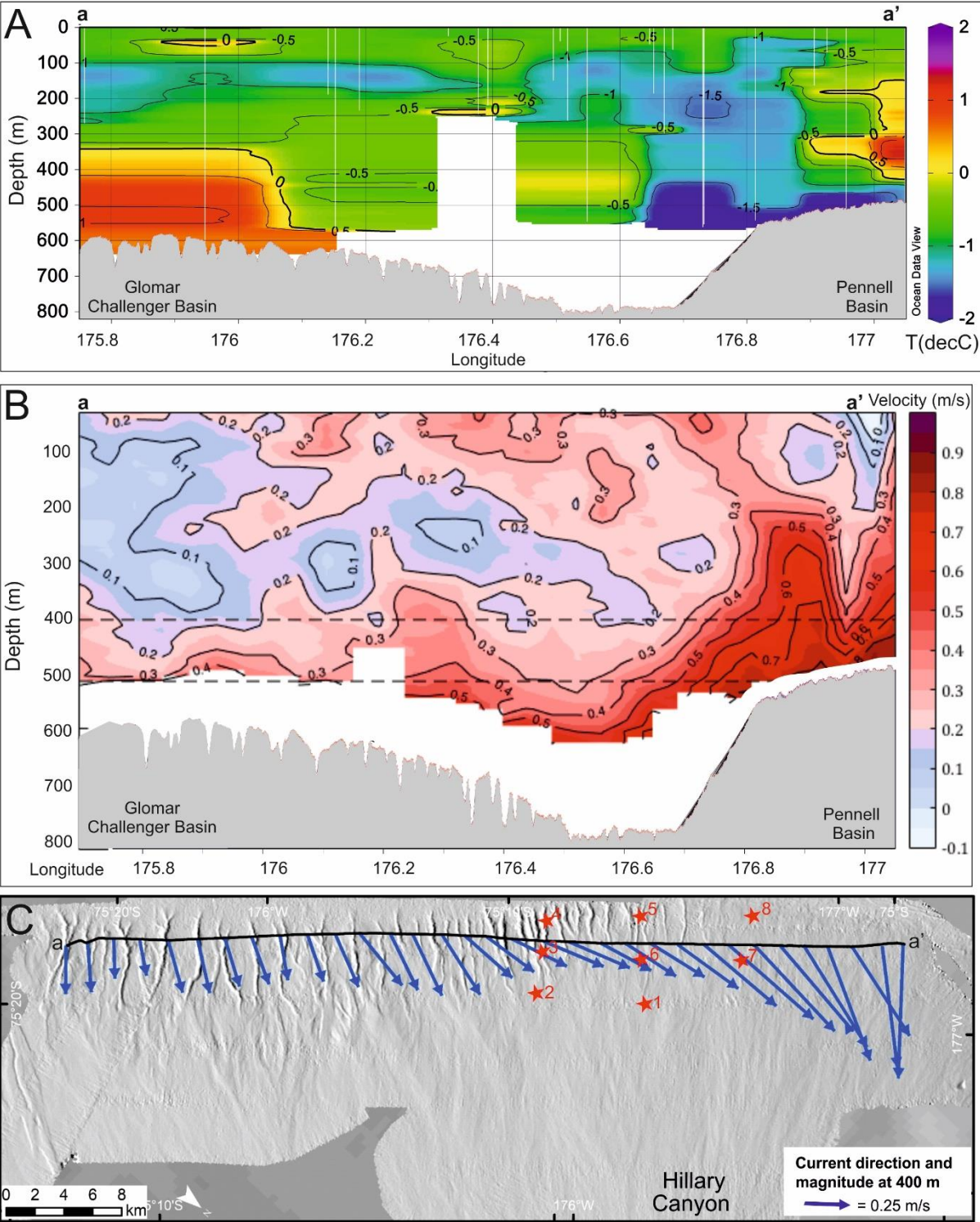
940

941

942

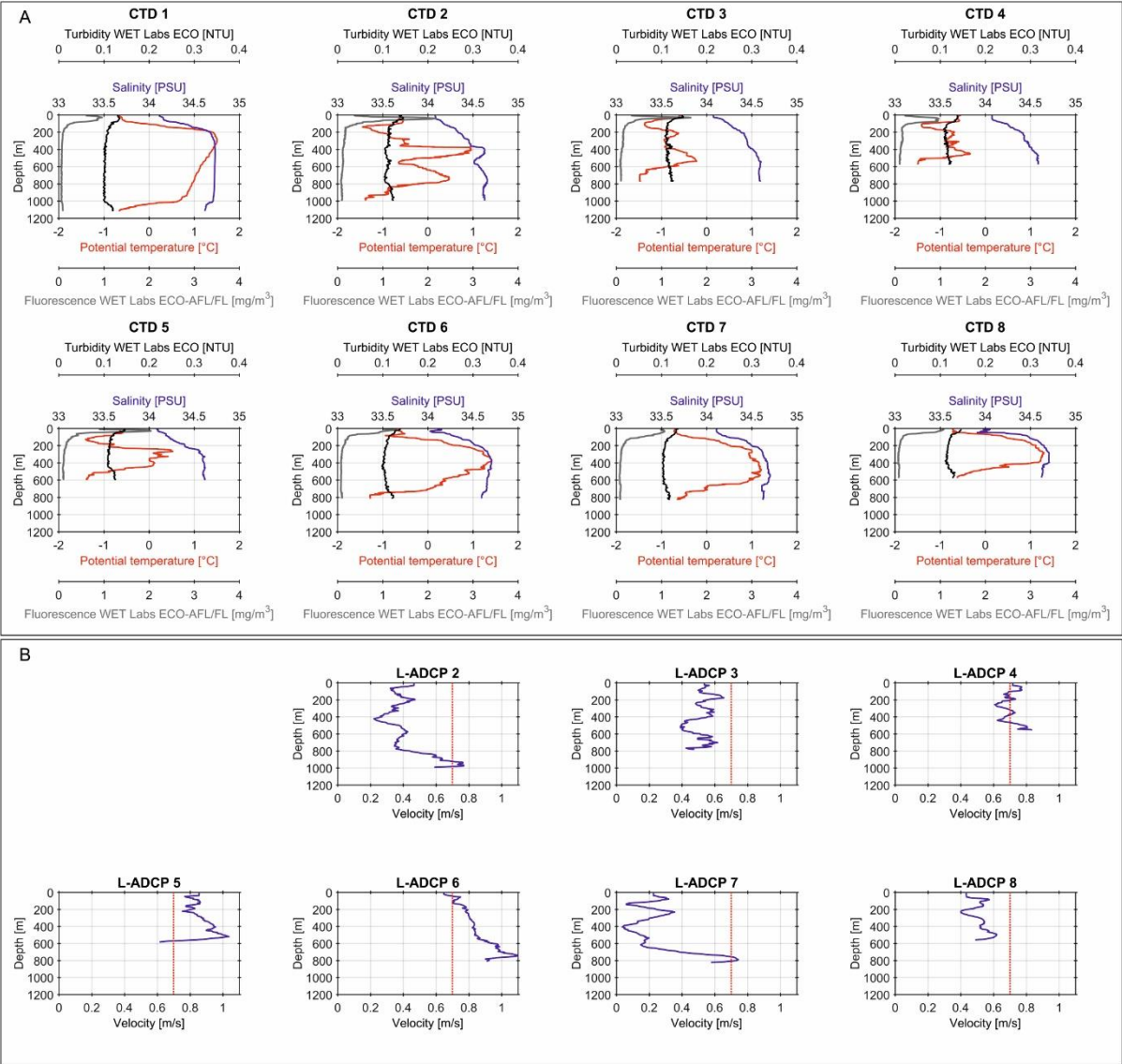
943 Figure 5







960 Figure 7



961

962

963

964

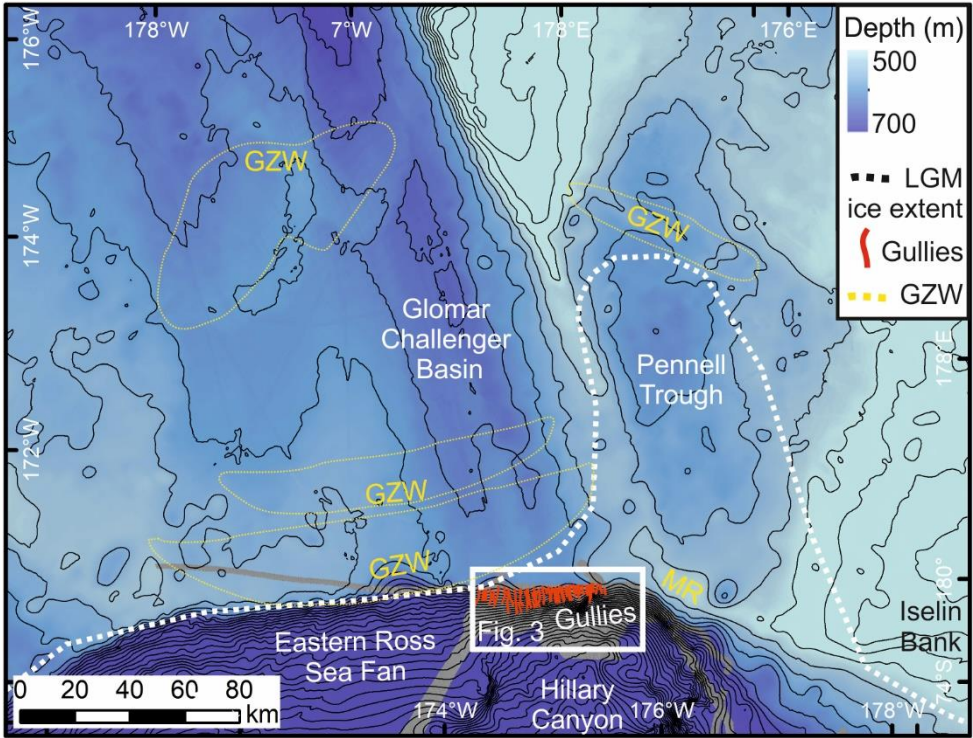
965

966

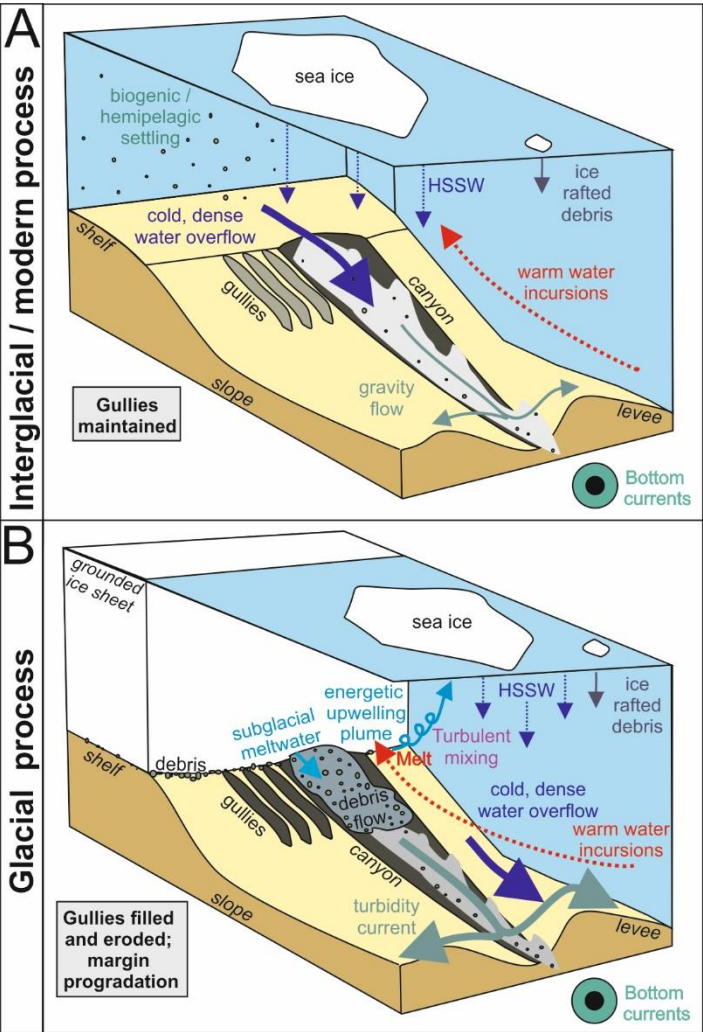
967

968

969 Figure 8.



982 Figure 9



983

984

985

986

987

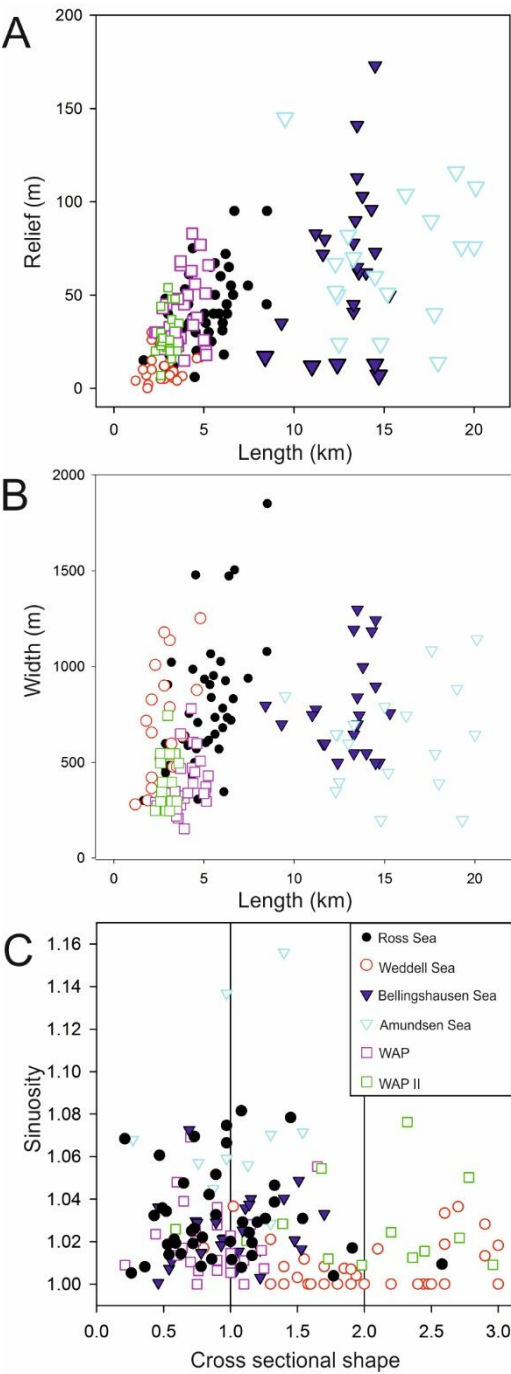
988

989

990

991

992 Figure 10



993

994

995

996

997

# 13. Supplementary Material – Figures

SM. Figure 1

